Geofísica Internacional (2025) **64-4**: 1781- 1802

# Analysis of flow Patterns and Hydrogeochemical Characteristics of Groundwater in a Volcanic Tectonic Basin

Leopoldo Gómez-Sandoval[1], Ruth Esther Villanueva-Estrada[2]*, Isabel Israde-Alcántara[3], Rafael Hernández-Guzmán[4], Jorge Alejandro Ávila-Olivera[3], Nora Elia Ceniceros Bombela[2] and María del Carmen Cano Correa[6]

## Abstract

This study uses physicochemical data and the geochemistry of major and minor ions to identify and describe groundwater flow patterns and hydrogeochemical characteristics in the Lake Cuitzeo basin. Located in the central-western region of Mexico, the basin is bounded by active faulting, subsidence, and hydrothermal activity along its margins. The study describes groundwater flow patterns, water types, water-rock interaction processes, and their relationship with geological faults traversed by the groundwater. Between 2022 and 2023, water quality was analyzed at 44 deep wells and seven springs. In situ measurements of physicochemical parameters were taken, and the concentrations of major and minor ions were plotted on D'Amore, Mifflin, and Piper diagrams. Seven hydrogeological environments were identified through which groundwater flows, promoting the weathering of Ca-Na-Mg silicates. Geological faults are directly related to flow directions, predominantly southwest-northeast. The primary recharge areas are located in the southwestern sector, where basic silicate rocks are dominant, leading to elevated $Mg^{2+}$ concentrations due to feldspar leaching. The predominant hydrogeochemical processes include silicate rock weathering, ion exchange, carbonation, water mixing, calcite precipitation, and gypsum dissolution. Three groundwater flow systems were identified: 82% of the flow is local, distributed throughout the basin; 16% is intermediate flow, concentrated in the central and northern areas; and 2% is deep circulation flow, found along the southern margin of the lake.

**Key words:** Water families, Lake Cuitzeo, central Mexico, volcanic environment, silicate weathering.

## Resumen

Este estudio tiene como objetivo utilizar datos fisicoquímicos y la geoquímica de iones mayores y menores para identificar y describir los patrones de flujo de agua subterránea y las características hidrogeoquímicas en la cuenca del Lago Cuitzeo. Ubicada en la región centro-occidental de México, la cuenca está delimitada por fallas activas, subsidencia y actividad hidrotermal a lo largo de sus márgenes. El estudio describe los patrones de flujo de agua subterránea, los tipos de agua, los procesos de interacción agua-roca y su relación con las fallas geológicas que atraviesa el agua subterránea. Entre 2022 y 2023, se analizó la calidad del agua en 44 pozos profundos y siete manantiales. Se realizaron mediciones in situ de los parámetros fisicoquímicos y se graficaron las concentraciones de iones mayores y menores en los diagramas de D'Amore, Mifflin y Piper. Se identificaron siete ambientes hidrogeológicos a través de las cuales fluye el agua subterránea, promoviendo la meteorización de silicatos Ca-Na-Mg. Las fallas geológicas están directamente relacionadas con las direcciones de flujo, predominantemente de suroeste a noreste.
Las principales áreas de recarga se encuentran en el sector suroeste, donde predominan las rocas de silicato básicas, lo que lleva a concentraciones elevadas de $Mg^{2+}$ debido al lixiviado de feldespato. Los procesos hidrogeoquímicos predominantes incluyen la meteorización de roca silicatada, el intercambio iónico, la carbonatación, la mezcla de aguas, la precipitación de calcita y la disolución de yeso. Se identificaron tres sistemas de flujo de agua subterránea: el 82% del flujo es local, distribuido por toda la cuenca; el 16% es flujo intermedio, concentrado en las áreas central y norte; y el 2% es flujo de circulación profunda, encontrado a lo largo del margen sur del lago.

**Palabras clave:** Familias de agua, Lago de Cuitzeo, centro de México, ambiente volcánico, meteorización de silicatos.

Received: January 23, 2025; Accepted: July 9, 2025; Published on-line: October 1, 2025.

Editorial responsibility: Dra. María Vicenta Esteller-Alberich

* Corresponding author: Ruth Esther Villanueva Estrada, ruth@igeofisica.unam.mx
[1] Universidad Michoacana de San Nicolás de Hidalgo, Programa Institucional de Doctorado en Ciencias Biológicas, , C.P. 58330 Morelia, Michoacán, México.
[2] Universidad Nacional Autónoma de México, Instituto de Geofísica, Unidad Michoacán, Km 8 Antigua carretera a Pátzcuaro 8701, Col. Ex Hacienda de San José de la Huerta, Morelia, Michoacán, C.P. 58190, México.
[3] Universidad Michoacana de San Nicolás de Hidalgo, Instituto de Investigaciones en Ciencias de la Tierra, , Santiago Tapia 403, 58000, Morelia, Michoacán, México.
[4] Universidad Michoacana de San Nicolás de Hidalgo, CONAHCYT-Instituto de Investigaciones sobre los Recursos Naturales, , C.P. 58330 Morelia, Michoacán, México.
[5] Organismo Operador de Agua Potable, Alcantarillado y Saneamiento de Morelia, Av. Rey Tanganxuan II 695, Col. Vista Bella, 58090, Morelia, Michoacán.
[6] Organismo Operador de Agua Potable, Alcantarillado y Saneamiento de Morelia, Morelia, Michoacán, México.
Leopoldo Gómez-Sandoval, Ruth Esther Villanueva-Estrada, Isabel Israde-Alcántara, Rafael Hernández-Guzmán, Jorge Alejandro Ávila-Olivera, Nora Elia Ceniceros Bombela, María del Carmen Cano Correa

https://doi.org/10.22201/igeof.2954436xe.2025.64.4.1857

## 1. Introduction

Groundwater extraction is globally significant, providing 50% of water for domestic use and 25% for agricultural irrigation, watering 38% of the world's crops (UNESCO, 2022). However, overexploitation can result in subsidence, declining piezometric levels, and water quality degradation (Burri *et al.*, 2019; Bagheri-Gavkosh *et al.*, 2021). In Mexico, 41% of aquifers are overexploited or deficiency of water availability (CONAGUA, 2021). Understanding the origin, flow, and vulnerability of these resources under anthropogenic pressure is crucial for sustainable management (Wang *et al.*, 2015).

Groundwater acquires its chemical composition through interactions with the rocks it traverses (Freeze and Cherry, 1979). Flow systems act as a transport mechanism, distributing these chemical interactions and forming spatial patterns within a basin (Toth, 1999). Chemical reactions such as dissolution/precipitation, oxidation/reduction, ion exchange, and mixing processes release specific elements into the water (Glynn and Plummer, 2005). These interactions, combined with groundwater movement driven by the subsurface configuration and geological structures, such as faults, define the hydrogeochemical characteristics of a region (Toth, 1999).

The integration of hydrogeochemistry with the groundwater flow system, initially introduced by (Toth, 1963), has become a fundamental tool in hydrogeology. This approach provides insights into hydrogeochemical processes, water families, and the hydrogeological environments shaping water composition.

The analysis of major ions has been proven effective in understanding hydrological dynamics in tectonic basins with high water demand, both in various regions of Mexico (Roy *et al.*, 2021; Amézaga-Campos *et al.*, 2022; Ramos-Leal *et al.*, 2018), and globally (Negrel *et al.*, 2011; Hartanto *et al.*, 2022; Gómez-Moncada *et al.*, 2022). Among the geological factors influencing groundwater geochemistry, fault systems play a key role due to their structural and hydraulic characteristics (Chihi *et al.*, 2015). Geologically, faults create discontinuities in flow patterns that promote water mixing and diverse water types due to the transport of dissolved species (Das *et al.*, 2020). Hydraulically, faults enhance permeability facilitating the upflow of deep groundwater (Yang, 2019).

In the Lake Cuitzeo basin, previous studies have primarily examined the geochemistry of geothermal zones in the northern basin (Alfaro *et al.*, 2002; Segovia *et al.*, 2005; 2010; Gómez-Cruz, 2020; Pérez-Martínez *et al.*, 2021) and groundwater flow patterns in the central-southwestern region (Garduño-Monroy *et al.*, 2014; Pérez-Villareal, 2018). However, these studies have not addressed the interplay between flow dynamics and hydrogeochemical characteristics at a basin-wide scale. This study fills that gap by integrating a detailed analysis of groundwater flow patterns and hydrogeochemical properties within a volcanic-tectonic basin context. By utilizing data collected over two years across different seasons, this research captures spatial and temporal variations in groundwater movement and chemical composition, offering new insights into the hydrogeological behavior of the basin. The results enhance our understanding of recharge areas, flow paths, and water-rock interactions, providing essential information for the sustainable management of groundwater resources in the region.

These findings are especially significant in the context of the Lake Cuitzeo basin, where the high degree of fracturing and diverse lithologies (Gómez-Vasconcelos *et al.*, 2021) create conditions for varied hydrogeochemical processes and flow patterns. These dynamics are particularly relevant given the subsidence issues (Figueroa-Miranda, 2018) and a groundwater deficit of -39,897,596 m³/year (CONAGUA, 2024b) in a region supporting over one million inhabitants. In this context, the present research aims to use physicochemical data and the geochemistry of major ions from wells and springs to identify and describe groundwater flow patterns, water types, water-rock interaction processes, and the hydrogeological environments influencing the volcanic Lake Cuitzeo basin in central Mexico.

By identifying vulnerable recharge zones and their relationship with geological structures and anthropogenic activity, this study offers relevant information for water resource planning and risk mitigation in the region. The proposed hydrogeochemical framework can support decision-making related to sustainable groundwater extraction and land use.

## 2. Study Area

### *2.1 Climate and Geology*

Lake Cuitzeo is located in an endorheic tectonic depression and covers approximately 4,025 km² (Hernández-Guzmán *et al.*, 2021). Its altitudinal gradient ranges from 1,767 to 3,426 meters above sea level (Figure 2) shaping diverse climatic and ecological conditions. The mean annual temperature is 17.4°C, and the average annual precipitation varies geographically. In the northern basin, precipitation ranges from 601 to 800 mm/year, whereas in the southern sector, it increases to 801–1,000 mm/year (CONAGUA, 2024c). The region exhibits two climate types: Cwb (temperate with dry winters and warm summers), predominant across most of the basin, and Cwa (temperate with dry winters and hot summers), mainly in the northwest (Beck *et al.*, 2018).

Geologically, the basin spans the states of Michoacán and Guanajuato in central Mexico, and began forming in the Middle Miocene, approximately 8 million years ago (Israde-Alcántara and Garduño-Monroy, 1999). It is part of the Trans-Mexican

Volcanic Belt (TMVB), a geologic province shaped by the subduction of the Cocos and Rivera plates beneath the North American plate along the Middle American Trench (Gómez-Vasconcelos *et al.*, 2021).

The Lake Cuitzeo basin hosts over 50 volcanic structures (Figure 1) displaying a wide range of geomorphic forms, including scoria cones, lava cones, semi-shield volcanoes, and fissure-fed lava flows (Gómez-Vasconcelos *et al.*, 2021). These volcanic features are integral to the basin's geology, influencing aquifer configuration, groundwater flow, and water-rock interactions.

In addition to their morphological diversity, these structures are composed of volcanic rocks with varying chemical compositions that shape hydrogeological processes throughout the basin. In the southwestern sector of the Lake Cuitzeo basin, basalts and basaltic andesites are found, representative of mafic rocks (Cardona-Melchor, 2015).

In the Sierra de Mil Cumbres, located in the southeastern part of the basin, intermediate rocks predominate, with andesites being the most abundant in the sequence; however, felsic rocks such as rhyolites are also present (Gómez-Vasconcelos, 2015). To the west lies the Quinceo volcano, composed of andesite of clearly intermediate composition, and the Tetillas volcano, whose lavas range from basaltic andesite to andesite, reflecting a transition from mafic to intermediate composition (Avellán *et al.*, 2020). Finally, in the southwestern portion of the lake (central portion of the basin), rock units of intermediate to mafic composition have been identified, consisting of ignimbrites associated with lava flows (Trujillo-Hernández *et al.*, 2022).

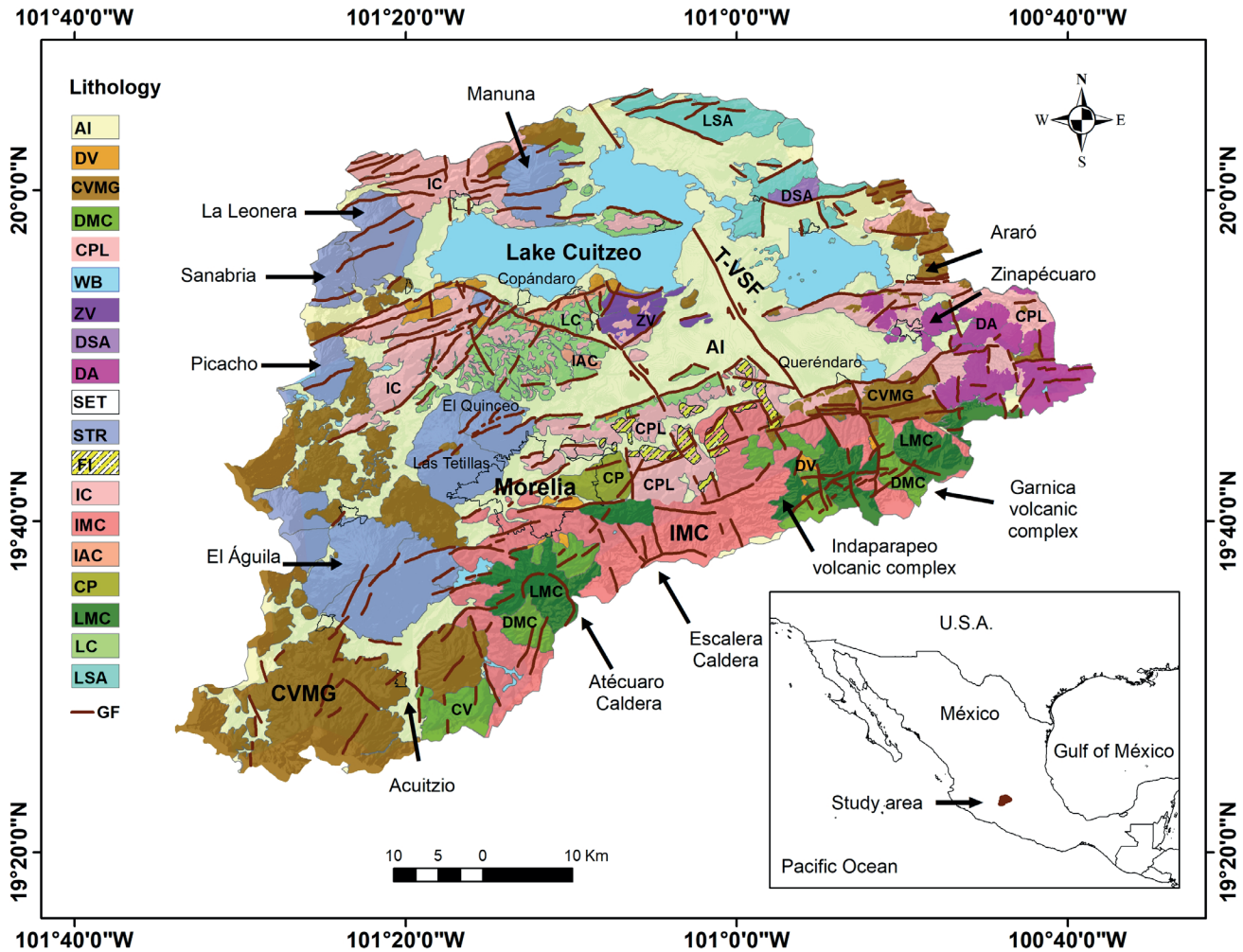


**Figure 1.** Geological map of the Lake Cuitzeo basin. Key: Al, Alluvium; DV, lahars, avalanches, and landslides; CVMG, Michoacán-Guanajuato Volcanic Field (4.7–0.02 Ma); DMC, Mil Cumbres Domes (23–14.1 Ma); CPL, Pumice Fall, Alegría, and lahars (1.5 Ma); WB, Water bodies; ZV, Zapata Volcano (8.1 Ma); DSA, San Andrés Diorite (14 Ma); DA, Araró Domes (1.3–1.03 Ma); SET, Settlements; STR, Stratovolcanoes; Fl, Fluviolacustrine (8 Ma); IC, Cuitzeo Ignimbrites (17.1 Ma); IMC, Mil Cumbres Ignimbrites (22.9–16.3 Ma); IAC, Ancient Cuitzeo Ignimbrites; CP, Punhuato (16.9 Ma); LMC, Mil Cumbres Lavas (23.1–21.5 Ma); LC, Cuitzeo Lavas (18.9–17.7 Ma); LSA, San Andrés Lavas (15.8–11.5 Ma); GF, Faults and alignments.

### *2.2 Hydrogeological and hydrogeochemical framework*

The Lake Cuitzeo basin forms part of Hydrological Region 12, Lerma-Chapala-Santiago, a critical water system in central Mexico. At the center of the basin lies the Morelia-Queréndaro Irrigation District, where agricultural and urban water demands are concentrated. According to the latest census conducted in 2007, 986 wells were recorded in the region, with water usage distributed between agricultural purposes (53.69%) and urban consumption (40.21%), leading to a significant water deficit of -39,897,596 m³/year (CONAGUA, 2024b).

Hydrogeochemically, the shores of Lake Cuitzeo exhibit diverse water facies, including bicarbonate, sulfate, and chloride water types, influenced by mixing processes and hydrothermal activity (Segovia *et al.*, 2005; 2010). Rapid spring recharge has been documented in some areas (Alfaro *et al.*, 2002), while precipitation of minerals of hydrothermal origin has been reported near geothermal zones (Segovia *et al.*, 2010; Pérez-Martínez *et al.*, 2021).

The northeastern sector of the basin is characterized by deep hydrothermal flows that ascend to the surface through geological fault system facilitating water-rock interactions and the thermal gradients (Pérez-Martínez *et al.*, 2021). In contrast, the southwestern part of the basin exhibits three distinct groundwater flow systems, where flow directions align with the regional topography (Pérez-Villareal, 2018). Meanwhile, in the central basin, a significant decline in piezometric levels has been reported attributed to over extraction and local geological conditions (Garduño-Monroy *et al.*, 2014).

### *2.3 Aquifer characteristics*

The geometry of the aquifer is shaped by the tectonic depression formed by the SW-NE fault system (CONAGUA, 2024b). Groundwater flows through two primary mediums: porous and fractured (CONAGUA, 2007). The porous medium predominates in the upper portion of the aquifer, while the fractured medium is characteristic of the lower portion (CONAGUA, 2020; 2024b). Together, these two media constitute a single hydrogeological unit with moderate to high permeability making the aquifer productive (CONAGUA, 2020). It is classified as heterogeneous, anisotropic, and predominantly unconfined, with localized semi-confined conditions (CONAGUA, 2020).

The porous medium corresponds to the lacustrine sequence of the basin, which has accumulated due to volcanic activity since the Late Miocene (Israde-Alcántara *et al.*, 2010). Successive monogenetic volcanism within the Cuitzeo graben was followed by lacustrine sedimentation, which reaches over 500 meters in thickness at the basin's center. This sedimentation is primarily composed of clays, silts, diatomites, and interbedded layers of sandstones and conglomerates, covered by pyroclastic deposits (Israde-Alcántara *et al.*, 2010).

In contrast, the fractured medium is predominantly formed by volcanic rocks such as basalts and tuffs, exhibiting both primary and secondary permeability (CONAGUA, 2020). Two major fault systems influence groundwater flow: the ENE-WSW faults of the Morelia-Acambay Fault System (MAFS) and the NNW-SSE faults associated with the Basin and Range system (Gómez-Vasconcelos *et al.*, 2021).

The aquifer´s composition varies across the basin. In the western region, pumice tuffs with interbedded lithic and clayey layers are prevalent, influenced by W-E fault systems. In the Álvaro Obregón and Queréndaro areas, the aquifer is dominated by clastic sediments such as gravels and sands. Closer to Lake Cuitzeo, it transitions to finer-grained materials, including clays, andesitic breccias, basalts, and basaltic ashes (CONAGUA, 2020; 2024b).

## 3. Methodology

### *3.1 Fieldwork*

Water samples were collected from 51 sites in the Lake Cuitzeo basin, comprising seven springs and 44 wells across 17 municipalities (Figure 2). In Morelia, 23 sampling points were analyzed (P-01 to P-19, P-44, M-01, M-06, and M-07), including three rural locations: Iratzio (P-41), Cuto de la Esperanza (P-42), and Atécuaro (M-04). The remaining sites were distributed across the following municipalities: Huiramba (P-20), Acuitzio (P-21, M-02), Tarímbaro (P-22, P-23), Charo (P-24, P-25), Álvaro Obregón (P-26, P-27), Copándaro (P-28, P-29, M-03), Chucándiro (P-30), Cuitzeo del Porvenir (P-31, P-32), Villa Morelos (P-33), Huandacareo (P-34), Santa Ana Maya (P-35, P-36), Zinapécuaro (P-37, P-38), Queréndaro (P-39), Indaparapeo (P-40), Lagunillas (M-05), and Pátzcuaro (P-43).

The 51 sites were sampled during both the rainy and dry seasons of 2022, and again during the same seasons in 2023, resulting in four samples per site and a total of 204 water samples collected. At each site, physicochemical parameters (pH, electrical conductivity, and discharge temperature) were measured in situ using a portable electronic multiparameter device (HANNA, model HI98129). Before each measurement, the instrument was calibrated for pH using certified buffer solutions of 4.01 and 7.01 and an electrical conductivity standard of 12,880 µS/cm. Subsequently, three water samples were collected in high-density polyethylene containers for chemical analyses of major and minor anions, cations, and trace elements. For the analysis of cations and trace elements, the samples were acidified in the field with 65.7% analytical-grade nitric acid to a pH of ~2. Samples

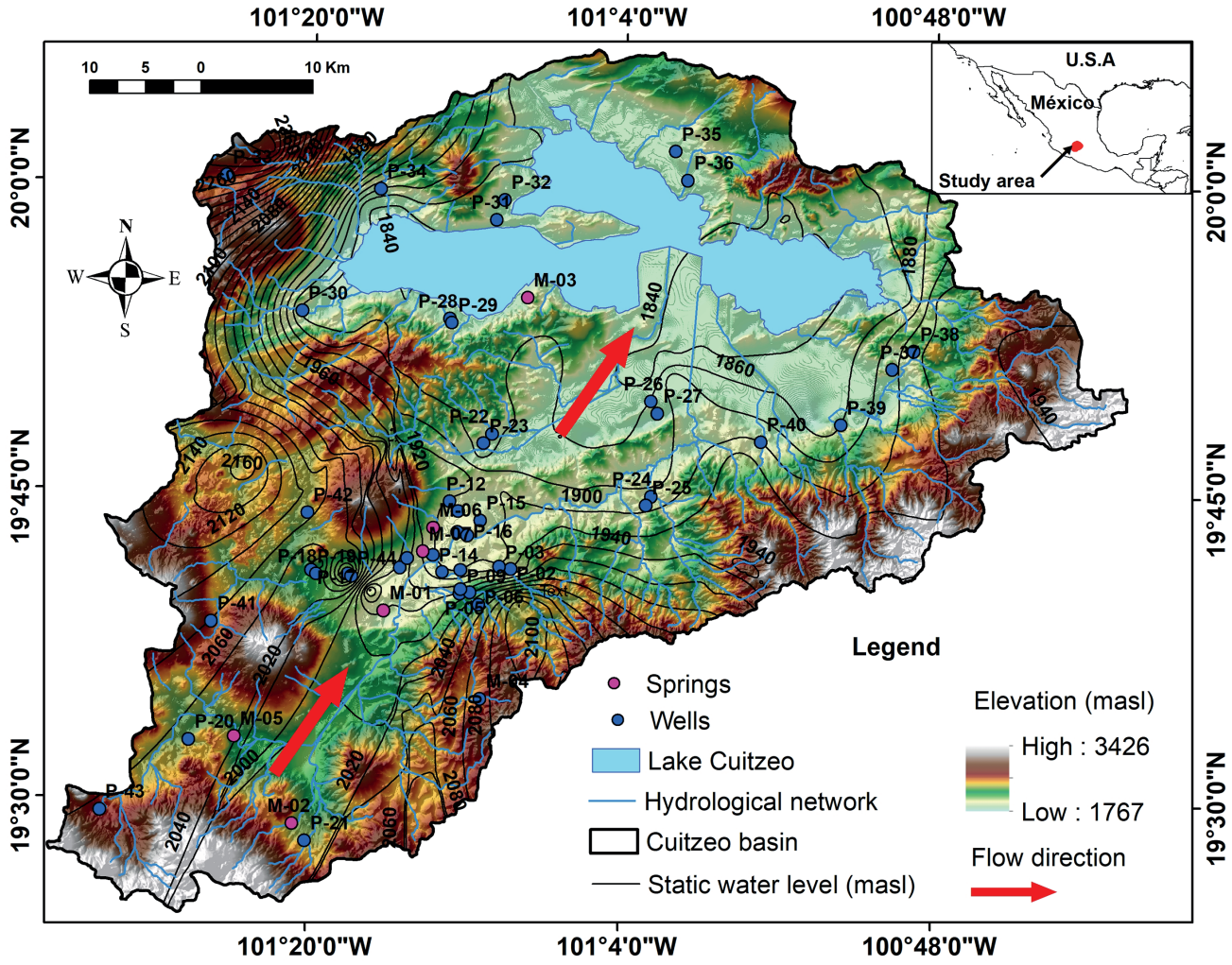


**Figure 2.** Location of wells and springs sampled in the basin, water resources, elevation (m.a.s.l.), static water level (CONAGUA, 2007), and flow direction (Garduño-Monroy *et al.*, 2014).

were transported in an insulated container with ice packs to the laboratory, where they were refrigerated at approximately 4 °C until chemical analysis.

Sampling was carried out following Section 7 of the Mexican Official Standard NOM-230-SSA1-2002, *Environmental Health. Water for human use and consumption — Sanitary requirements to be met by public and private supply systems during water handling. Sanitary procedures for sampling*. The analysis of major ions and metals was carried out immediately after delivery to the laboratory.

### *3.2 Laboratory work*

Chemical analysis of major and minor ions ($Li^+$, $Na^+$, $K^+$, $Ca^{2+}$, $Mg^{2+}$, $F^-$, $Cl^-$, $SO_4^{2-}$) was performed using ion chromatography with a conductivity detector and suppressor on a Thermo Scientific ICS-5000+DP system. Quality control was ensured through the periodic injection of a standard solution after every 10 samples, allowing verification of the instrument's response stability throughout the analytical sequence. The analysis of $CO_3^{2-}$ and $HCO_3^-$ ions was conducted through volumetric titration with visual indicators, using HCl solutions previously standardized with a primary standard. Aluminum (Al) and silicon (Si) analyses were carried out using inductively coupled plasma optical emission spectrometry (ICP-OES) on an Agilent 5100 SVDV instrument. These chemical analyses were performed at the Geochemical Laboratory for Geothermal Fluids of the Geophysics Institute, Morelia Unit, UNAM.

### *3.3 Data processing*

The ionic charge balance was performed on a total of 204 water samples to evaluate the electroneutrality error, with an acceptable threshold of ±10% (Hem, 1985). To classify ground-

water flow systems, the Mifflin (1988) methodology was applied. This approach is based on the ionic relationship $Na^+ + K^+$ vs. $Cl^- + SO_4^{2-}$, which allows the identification of flow types: recent infiltration, intermediate, and deep circulation.

Additionally, the processes of water-rock interaction that shape the water chemistry in the Lake Cuitzeo basin were evaluated using the D'Amore diagram (D'Amore *et al.*, 1983). This diagram utilizes the concentration of water samples (meq/L), where parameters A-F are normalized between +100 and -100. Σ(+) and Σ(-) represent the sum of cations and anions, respectively, in meq/L. The equations used to construct this diagram are as follows:

$$\frac{100}{\sum[-]} \times ([HCO_3^-] - [SO_4^{2-}]) \rightarrow\rightarrow Equation\ [A]$$

$$100 \times \left(\frac{[SO_4^{2-}]}{\sum[-]} - \frac{[Na^+]}{\sum[+]}\right) \rightarrow\rightarrow Equation\ [B]$$

$$100 \times \left(\frac{[Na^+]}{\sum[+]} - \frac{[Cl^-]}{\sum[-]}\right) \rightarrow\rightarrow Equation\ [C]$$

$$100 \times \left(\frac{[Na^+] - [Mg^{2+}]}{\sum[+]}\right) \rightarrow\rightarrow Equation\ [D]$$

$$100 \times \left(\frac{[Ca^{2+}] + [Mg^{2+}]}{\sum[+]} - \frac{[HCO_3^-]}{\sum[-]}\right) \rightarrow\rightarrow Equation\ [E]$$

$$100 \times \left(\frac{[Ca^{2+}] - [Na^+] - [K^-]}{\sum[+]}\right) \rightarrow\rightarrow Equation\ [F]$$

The water type was classified using the diagram proposed by Piper (1944), created with the Diagrammes v6.77 software. To determine saturation indices and establish aqueous species and minerals under equilibrium conditions, the PHREEQC Interactive software (version 3.3.7-11094) was employed, utilizing the PHREEQC.DAT database.

To visualize regional trends in the concentrations of certain elements, the results were mapped using the Inverse Distance Weighted (IDW) interpolation technique in ArcMap 10.8. This technique assumes that elements closer to each other are more similar, assigning higher weights to values near the prediction location (Esri, 2024).

## 4. Results

### *4.1 Descriptive hydrogeochemical characterization of groundwater and springs*

A total of 204 water samples were analyzed to evaluate their physicochemical characteristics and ionic composition. An ionic charge balance was performed to assess the electroneutrality error, with an acceptable threshold of ±10% (Hem, 1985). Eight samples exceeded this limit and were therefore excluded from further ionic analyses. Consequently, 196 valid samples were included in the hydrogeochemical analysis.

Descriptive statistics for major hydrogeochemical parameters are presented in Table 1, and their distribution is illustrated through boxplots in Figure 3. The analysis was conducted in accordance with the Mexican drinking water standard NOM-127-SSA1-2021.

#### 4.1.1 Physicochemical parameters

Water temperatures range from 15.9 °C to 49.0 °C (average 25.1 °C), exceeding the basin's annual mean of 17.4 °C. The highest values were recorded at thermal spring M-03 and site

**Table 1.** Descriptive statistics of the hydrogeochemistry of sampled wells and springs. Data below the limit of quantification (LQ), as well as cases in which the chemical species were not present (carbonates and bicarbonates), were excluded. All samples were included for the analysis of physicochemical parameters. Analytical precision for ion chromatography was as follows: $Li^+$ (0.6%), $Na^+$ (0.8%), $K^+$(1%), $Ca^{2+}$ (0.2%), $Mg^{2+}$ (0.5%), $F^-$ (0.2%), $Cl^-$ (0.07%), and $SO_4^{2-}$ (0.2%).

| | $Li^+$ (mg/L) | $Na^+$ (mg/L) | $K^+$ (mg/L) | $Ca^{2+}$ (mg/L) | $Mg^{2+}$ (mg/L) | $F^-$ (mg/L) | $Cl^-$ (mg/L) | $SO_4^{2-}$ (mg/L) | $CO_3^{2-}$ (mg/L) | $HCO_3^-$ (mg/L) | T (°C) | EC µS/cm | pH |
|---|---|---|---|---|---|---|---|---|---|---|---|---|---|
| Descriptive statistics (n=204) | | | | | | | | | | | | | |
| Analyzed samples | 35 | 196 | 196 | 196 | 195 | 156 | 196 | 196 | 49 | 196 | 204 | 204 | 204 |
| Minimum | 0.007 | 5.48 | 1.67 | 1.68 | 0.278 | 0.064 | 0.39 | 0.48 | 2.88 | 70.11 | 15.9 | 140 | 6.3 |
| Maximum | 1.829 | 674.99 | 58.79 | 89.70 | 49.36 | 9.42 | 235.73 | 522.4 | 173.68 | 921.36 | 49 | 3180 | 9.2 |
| Mean | 0.223 | 71.40 | 7.29 | 26.76 | 14.68 | 0.52 | 22.55 | 31.98 | 22.03 | 252.65 | 25.1 | 596.1 | 7.4 |
| Q.L. | 0.007 | 0.20 | 0.42 | 0.27 | 0.19 | 0.06 | 0.36 | 0.1256 | NA | NA | NA | NA | NA |

<Q.L. = Quantification limit; NA = Not applicable;

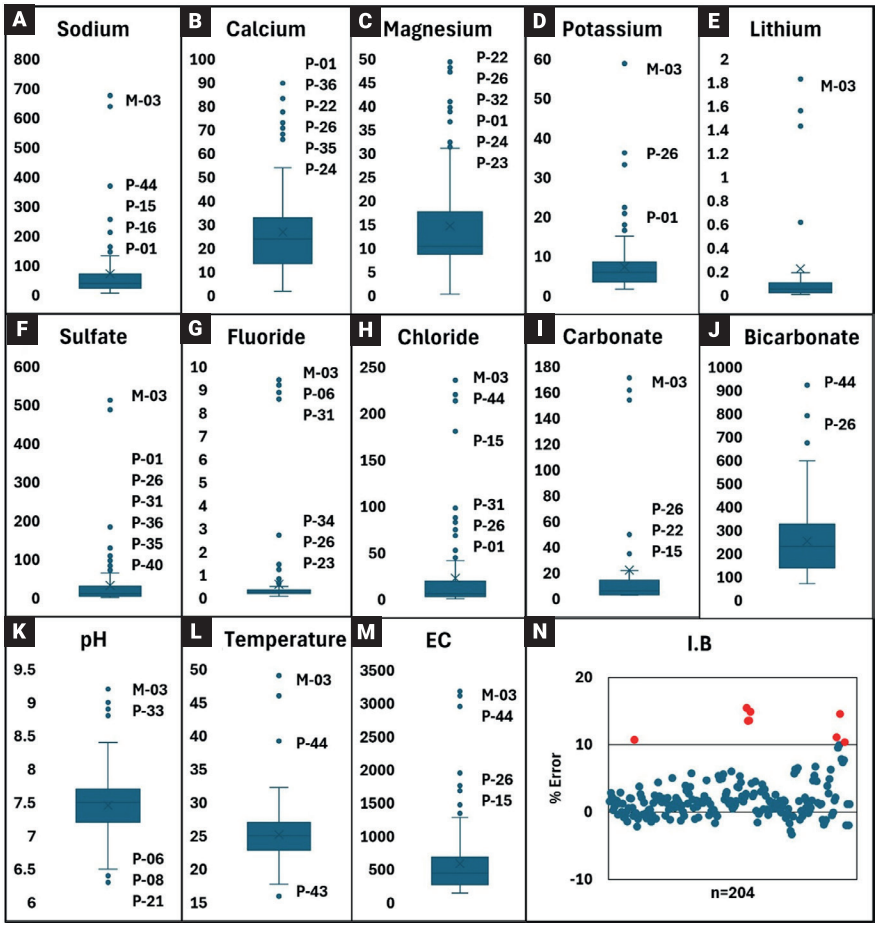


**Figure 3.** Boxplot of the measured variables, the concentration of ions $Na^+$ (n=196), $Ca^{2+}$ (n=196), $Mg^{2+}$ (n=195), $K^+$ (n=196), $Li^+$ (n=35), $SO_4^{2-}$ (n=196), $F^-$ (n=156), $Cl^-$ (n=196), $CO_2^-$ (n=49), $HCO_3^-$ (n=196), are in mg/L, temperature in °C, EC in µS/cm. The ion balance is in percentage (values in red were discarded for not meeting the quality criterion of ±10%).

P-44, while the lowest was observed at P-43 (Figure 3L). This variability reflects geothermal influence and local hydrogeological conditions. pH values range from 6.3 to 9.2 (average 7.4), with slightly alkaline conditions prevailing in the central and western zones, and more acidic values in the southwest, likely due to higher precipitation and subsequent $CO_2$ enrichment. Most samples fall within the limits established by NOM-127-SSA1-2021, except at sites M-03, P-06, P-08, P-21, and P-33. Electrical conductivity (EC) ranges from 140 to 3180 µS/cm (average 596.1 µS/cm). Nearly all samples comply with the potable water limit (EC < 2500 µS/cm), except for the thermal spring M-03. Higher EC values are concentrated near Lake Cuitzeo, whereas lower values predominate in the southwest.

### 4.1.2 Ionic parameters

Sodium concentrations range broadly (4.48 to 674.99 mg/L), with elevated values at M-03, P-01, P-15, P-26, and P-44, associated with halides, ion exchange, and thermal activity (Hounslow, 1995). Lower concentrations prevail in the southwest. Calcium (1.68 to 89.70 mg/L) and magnesium (0.278 to 49.36 mg/L) exhibit localized enrichment at sites influenced by carbonates, sulfates, and silicates. Site M-03 shows low magnesium, likely due to thermal precipitation processes (Case *et al.*, 2011). Potassium concentrations (1.67 to 58.79 mg/L) are generally low, with high values at M-03, P-01, and P-26, reflecting interaction with feldspars and micas (Hounslow, 1995).

Sulfate levels (0.48 to 522.4 mg/L) exceed the maximum permissible limit only at M-03 (Figure 3F), where thermal input and mineral interactions are evident. Lower sulfate concentrations are found in the southwest. Fluoride concentrations (0.064 to 9.42 mg/L) exceed permissible limits at M-03 and occasionally at P-06 and P-31, likely due to mineral desorption under alkaline conditions. Chloride ranges from 0.39 to 235.73 mg/L; low average concentrations contrast with high values at M-03, P-01, and P-26, indicating thermal and halide influence. High bicarbonate (70.11 to 921.36 mg/L) and carbonate (2.88 to 173.68 mg/L) concentrations occur at P-26, P-44, and M-03, correlating with

elevated EC and temperature. Lithium concentrations (0.007 to 1.829 mg/L) are generally low, with marked outliers at M-03 and P-44 (Figure 3E), suggesting influence from geological or evaporitic sources (Hounslow, 1995).

### *4.2 Geochemical modeling of the water equilibrium state*

The saturation indices (SI) of the mineral phases from wells and springs are shown in Figure 4. The SI indicates the thermodynamic state of minerals with respect to water: A SI $< 0$ indicates undersaturation, suggesting that minerals tend to dissolve, while an SI $> 0$ indicates supersaturation, indicating a tendency to precipitate depending on the physicochemical parameters; and SI $\approx 0$ ($\pm 0.5$) suggest a thermodynamic equilibrium with the water (Appelo and Postma, 2005).

The mineral phases identified in the basin include silicates, carbonates, halides, and sulfates. Supersaturated minerals which are likely to precipitate include olivine, Ca-montmorillonite, illite, kaolinite, K-feldspar, sepiolite, sepiolite (d), quartz, chalcedony, calcite, and alunite. On the other hand, undersaturated minerals which are prone to dissolution include albite, anorthite, silica, halite, anhydrite, and gypsum. Although the saturation index (SI) may indicate supersaturation, the precipitation of olivine and K-feldspar under natural environmental conditions is unlikely. This is due to their extremely slow reaction kinetics, the high nucleation barriers involved, and their tendency to transform into more stable secondary minerals. Consequently, these minerals typically dissolve rather than precipitate (Drever, 1997).

These results highlight the ongoing water-rock interactions within the basin. The dissolution of undersaturated minerals contributes to the groundwater's chemical composition. The spatial distribution of these processes will be discussed in relation to geological structures and hydrogeochemical zones.

### *4.3 Seasonal variation in ionic concentration*

Electrical conductivity (EC) was selected as a proxy for ionic concentration due to its sensitivity to hydrological processes (e.g., recharge and evaporation) and its capacity to reflect general water chemistry without requiring complex analysis. Although pH and temperature are relevant for hydrogeochemical interpretation, they are less responsive to seasonal variation and were therefore excluded from this section.

To evaluate seasonal variation, EC data were grouped by campaign: dry season 2022, rainy season 2022, dry season 2023, and rainy season 2023. The Shapiro-Wilk test showed p-values $< 0.05$ in all cases, rejecting the null hypothesis and confirming non-normal distribution. Therefore, the non-parametric Wilcoxon test was applied at a 95% confidence level.

In 2022, no significant differences were found between dry and rainy seasons ($p > 0.05$). In contrast, the 2023 data showed significant differences ($p < 0.05$), indicating seasonal effects in that year. These results suggest that EC variation was more strongly influenced by interannual differences—possibly linked to irregular precipitation—rather than by seasonal effects alone.

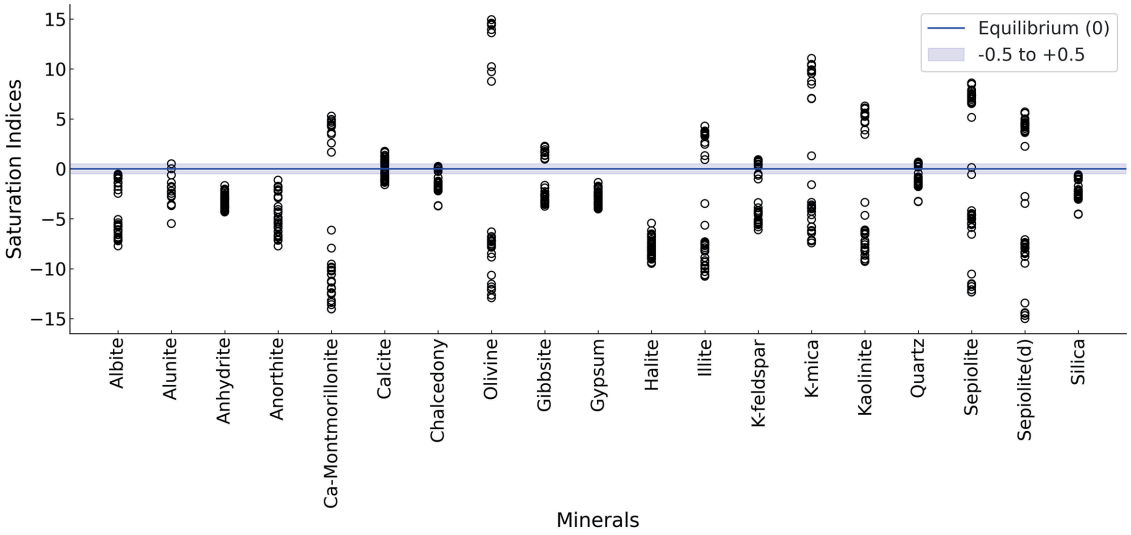


**Figure 4.** Saturation indices of mineral phases present in the Lake Cuitzeo basin.

## 5. Discussion

### *5.1 Water types in the basin*

According to the Piper diagram, all the groundwater and spring samples from the basin fall within the bicarbonate-type. A significant proportion (36.2%) of the samples exhibit a sodium-dominated chemistry (Na-$HCO_3$), while a smaller percentage (2.04%) is characterized by magnesium-dominated waters (Mg-$HCO_3$). The remaining 61.76% corresponds to waters whose chemistry reveals possible ion exchange processes or mixing with other types of waters, such as sulfate-rich waters.

The observed dominant cation exchange is consistent with the general groundwater flow direction in the basin, which follows a SW-NE gradient (Garduño-Monroy *et al.*, 2014). In the southwestern part of the basin, the dominant cation is magnesium ($Mg^{2+}$), which is progressively replaced by calcium ($Ca^{2+}$) toward northeast. In the northwest, $Ca^{2+}$ is predominantly replaced by sodium ($Na^{+}$) (Figure 5). This trend in cation exchange highlights the dynamic nature of the hydrogeochemical processes occurring within the basin (Figure 6).

### *5.2 Chemical indicators of water-rock interaction*

Geochemical analysis, together with site geology, saturation indices, Piper (1954), and D'Amore diagrams (D'Amore *et al.*, 1983), indicates that the nine water types (based on dominant cation) have circulated through seven distinct hydrogeological environments (Figure 5), distributed across the basin (Figure 7).

**Environment 1:** Mg–Ca waters and weathering of Mg-silicates

This environment, located mainly in the basin's southwest (Figure 6), produces Mg–$HCO_3$, Mg–Ca–$HCO_3$, and Ca–Mg–$HCO_3$ waters. The source rocks belong to the Michoacán-

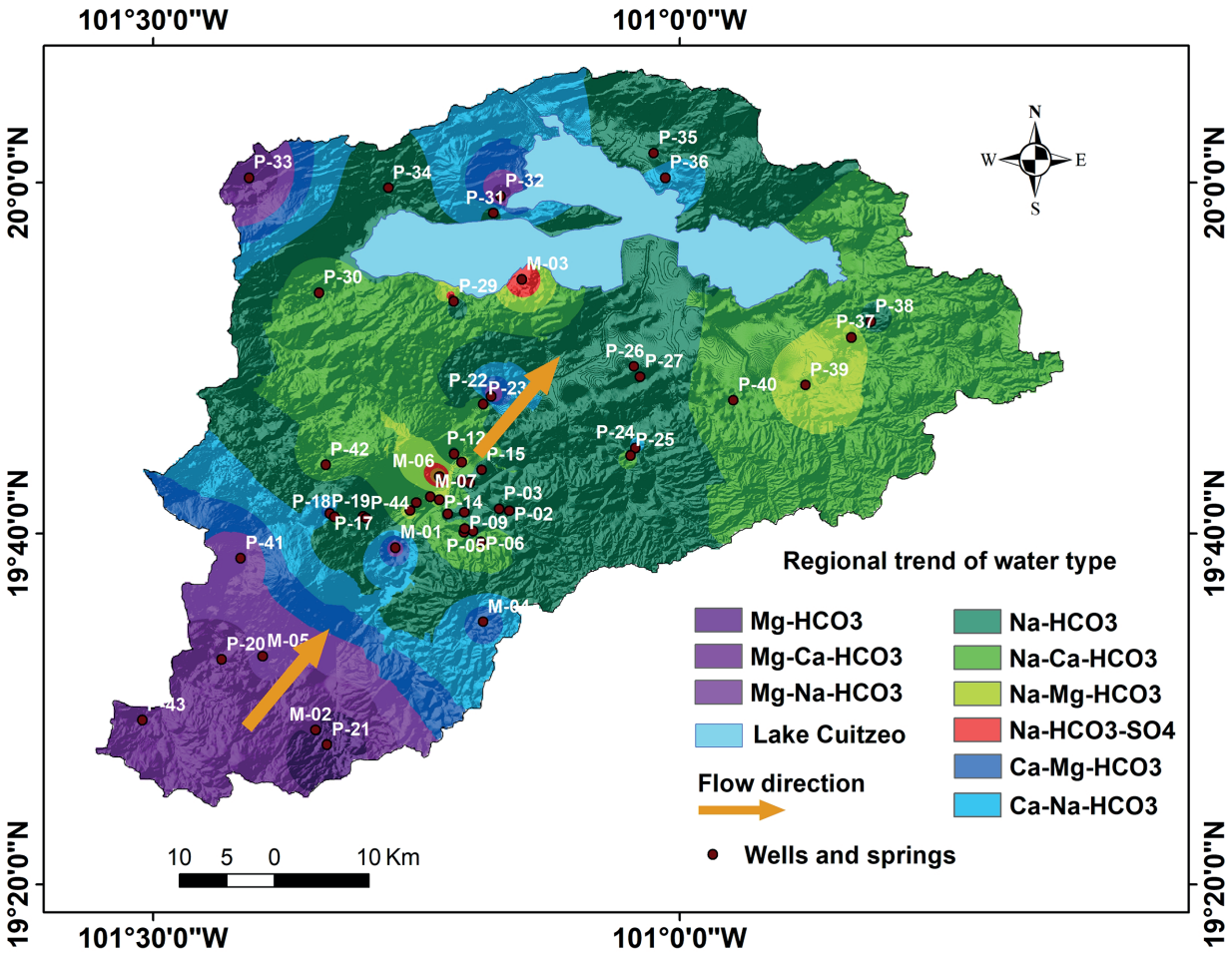


**Figure 5.** The regional trend of groundwater types was generated through interpolation of data from the sampling sites. Colors represent the water type, classified according to the dominant cation at each site. Arrows show the groundwater flow direction, based on Garduño *et al.* (2014).

Guanajuato Volcanic Field (MGVF), including the Nieve volcanic complex, dominated by basalts (Cardona-Melchor, 2015). This area reaches elevations of 3,426 m a.s.l. Waters circulate through clayey materials associated with the fluvio-lacustrine sequence (Equation B, methodology section).

Bicarbonate enrichment (Equation A) results from the dissolution of $CO_2$ incorporated by rainwater according to the following chemical equation (Appelo and Postma, 2005).

$$CO_2+H_2O\leftrightarrow H_2CO_3\leftrightarrow H^++HCO_3^-\rightarrow\rightarrow \textit{Reaction}\ [1]$$

These waters have neutral pH (~7.1) and low electrical conductivity (220 µS/cm). They are supersaturated with silicate minerals such as olivine, pyroxene, plagioclase, and amphibole (Cardona-Melchor, 2015). The observed $Ca^{2+}$ and $Mg^{2+}$ concentrations originate from silicate weathering (Equation D) of basic-composition rocks, rather than dolomitized limestone (D'Amore *et al.*, 1983). Based on SI values, $Ca^{2+}$ enrichment derives from weathering of Ca-montmorillonite and anorthite (Reaction 2; Appelo and Postma, 2005), while $Mg^{2+}$ comes from olivine (Reaction 3; Hounslow, 1995), illite, and sepiolite.

$$Ca(Al_2Si_2)O_8+2H^++H_2O\rightarrow Al_2Si_2O_5(OH)_4+Ca^{2+}\rightarrow\rightarrow \textit{Reaction}\ [2]$$

$$Mg_2SiO_4+4CO_2+4H_2O\rightarrow 2Mg^{2+}+4HCO_3^-+H_4SiO_4\rightarrow\rightarrow \textit{Reaction}\ [3]$$

Olivine and Ca-plagioclase are among the most weathering-prone minerals (Lewis *et al.*, 2021), explaining the enrichment of $Ca^{2+}$ and $Mg^{2+}$ in this environment.

**Environment 2:** Predominance of Mg–Na waters

Na–Mg–$HCO_3$ and Mg–Na–$HCO_3$ waters are found in the southwest-central zone, particularly in Morelia and Tarímbaro. These flows originate from volcanic formations such as El Águila, El Quinceo, and Las Tetillas (Figure 1), composed mainly of basaltic andesites (Avellán *et al.*, 2020). The water circulates through clayey materials of the fluvio-lacustrine sequence (Equation B).

Bicarbonate enrichment is driven by subsurface $CO_2$ incorporation (Equation A; Reaction 1). The volcanic rocks contain plagioclase, olivine, and pyroxene (Gómez-Vasconcelos *et al.*, 2015; Avellán *et al.*, 2020), making silicate weathering the primary source of dissolved ions. According to SI values, $Mg^{2+}$ enrichment results from olivine weathering (Reaction 3) in basic-composition rocks, while $Na^+$ originates from albite weathering (Hounslow, 1995), which also generates kaolinite supersaturation (Figure 4). These processes are summarized in Reaction 4.

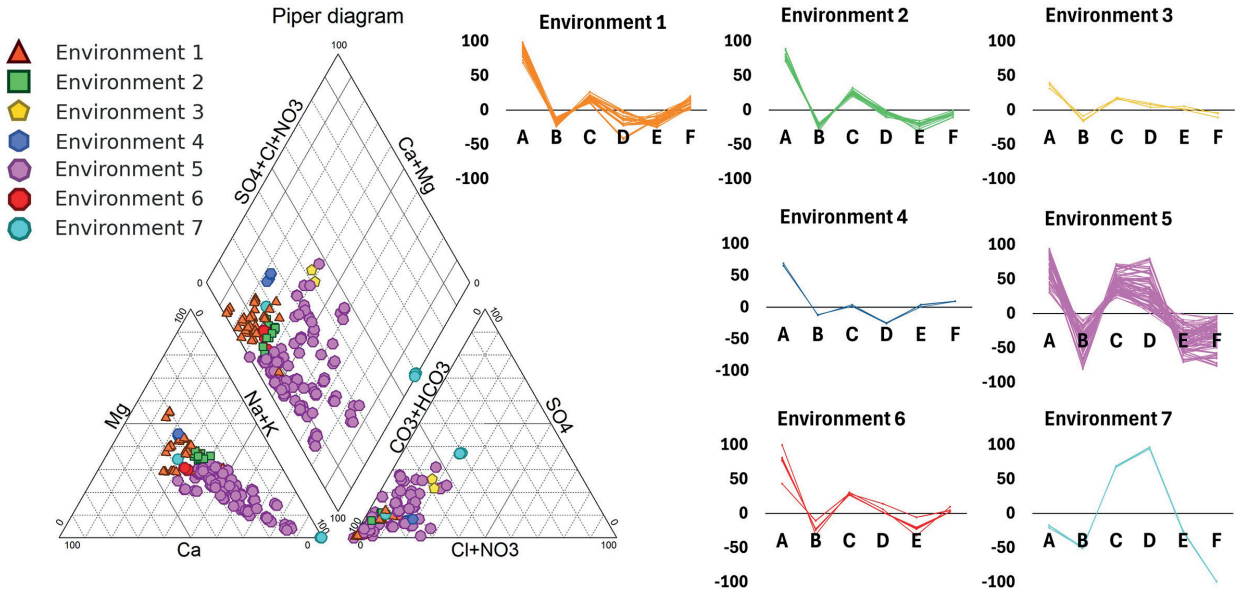


**Figure 6.** Right: D'Amore diagrams showing 196 groundwater samples, each represented by a line, allowing the identification of seven distinct hydrogeological environments. Environment 1: P-20, M-02, P-21, P-22, P-29, P-33, M-04, M-05, P-43. Environment 2: P-11, M-01, P-23, P-41. Environment 3: M-06. Environment 4: P-32. Environment 5: P-01, P-02, P-03, P-04, P-06, P-07, P-08, P-09, P-10, P-12, P-13, P-14, P-15, P-16, P-17, P-18, P-19, P-25, P-26, P-27, P-30, P-31, P-34, P-35, P-36, P-37, P-38, P-39, P-40, P-42, M-07, P-44. Environment 6: P-05, P-24. Environment 7: M-03. Left: In the Piper diagram, the symbols correspond to the hydrogeological environments, allowing for the visualization of the water type variability within each environment, as more than one water type may be present in a single category.

$2NaAlSi_3O_8 + 2CO_2 + 11H_2O \rightarrow Al_2Si_2O_5(OH)_4 + 2Na^+ + 2HCO_3^- + 4H_4SiO_4 \rightarrow \rightarrow$ *Reaction* [4]

**Environment 3:** Weathering of plagioclases with ion exchange

Na–Ca–$HCO_3$ water, represented by one site (M-06) in the southwest-central basin, flows through the Las Tetillas volcanism (Avellán *et al.*, 2020). Bicarbonate enrichment originates from $CO_2$ dissolution (Equation A; Reaction 1).

The volcanic rocks are rich in plagioclase, olivine, and pyroxene. $Ca^{2+}$ derives from weathering of Ca-silicates like anorthite (Reaction 2), and $Na^+$ from albite weathering (Reaction 4) in intermediate-composition rocks, which produces kaolinite and leads to groundwater supersaturation with this mineral (Figure 4). As water moves through clays of the fluvio-lacustrine sequence (Equation B), ion exchange enriches it in $Na^+$ (Reaction 5). Additionally, carbonation occurs (Equation E; Reaction 6), in an environment where calcite is undersaturated (SI = -0.68).

$Ca^{2+} + 2Na^+clay \leftrightarrow 2Na^+ + Ca^{2+}clay \rightarrow \rightarrow$ *Reaction* [5]

$HCO_3^- + H_2O \rightarrow H_3O + CO_3^- \rightarrow \rightarrow$ *Reaction* [6]

**Environment 4:** Calcareous carbonate with Mg-silicate weathering

Mg–Ca–$HCO_3$ water occurs at site P-32 in the fluvio-lacustrine sequence near the northern shore of Lake Cuitzeo. Bicarbonate enrichment arises from $CO_2$ dissolution (Equation A; Reaction 1), while $Ca^{2+}$ and $Mg^{2+}$ derive from weathering of anorthite and olivine (Equation D; Reactions 2 and 3). This environment is predominantly calcareous (Equation F) and exhibits calcite supersaturation (SI = 1.22), with minimal $Na^+$ interaction.

**Environment 5:** Predominance of Na with weathering of Ca–Mg silicates and ion exchange

Na–$HCO_3$ waters, along with smaller proportions of Na–Ca–$HCO_3$, Ca–Na–$HCO_3$, and Na–Mg–$HCO_3$, are widely distributed across the basin except in the southwest (Figure 6). These flows originate from the Mil Cumbres ignimbrites, El Quinceo lavas (Avellán *et al.*, 2020), and the fluvio-lacustrine sequence. Similar waters have been reported in the Araró-Simirao geothermal zone (Pérez-Martínez, 2021).

These waters are enriched in bicarbonates (Equation A; Reaction 1) and major cations ($Na^+$, $Ca^{2+}$, $Mg^{2+}$) as a result of silicate weathering processes occurring in rocks of intermediate composition (Hounslow, 1995). The local volcanism is rich in plagioclase, olivine, pyroxene, and amphibole (Gómez-Vasconcelos *et al.*, 2015). $Na^+$ enrichment comes from albite (Reaction 4), while $Ca^{2+}$ and $Mg^{2+}$ originate from anorthite and olivine (Reactions 2 and 3). Ion exchange with clays (Equation B) enhances sodium concentration (Reaction 5).

**Environment 6:** Ca–bicarbonate water and Na–Mg silicate weathering

Ca–Na–$HCO_3$ and Ca–Mg–$HCO_3$ waters appear at four sites in the basin's central region (Figure 6). They originate from ignimbrites of the Atécuaro and La Escalera calderas, and from the northern fluvio-lacustrine sequence. The volcanism is rich in plagioclase, olivine, pyroxene, sanidine, phlogopite, biotite, and hornblende (Gómez-Vasconcelos *et al.*, 2015).

These waters show bicarbonate enrichment (Equation A; Reaction 1), with $Ca^{2+}$ from anorthite (Reaction 2), $Mg^{2+}$ from olivine (Reaction 3), pyroxene, and biotite, and $Na^+$ from albite (Reaction 4). Ion exchange with clays further modifies the composition (Equation B; Reaction 5).

**Environment 7:** Evaporitic with calcite precipitation

Na–$HCO_3$–$SO_4$ water from a thermal spring (M-03) near Copándaro results from mixing deep sulfate-rich and shallow bicarbonate waters (Segovia *et al.*, 2005). Sulfates originate from gypsum (Equation A), documented in Lake Cuitzeo sediments (Israde-Alcántara *et al.*, 2010), through the following reaction (Freeze and Cherry, 1979):

$CaSO_4: 2H_2O \rightarrow Ca^{2+} + SO_4^{2-} + 2H_2O \rightarrow \rightarrow$ *Reaction* [7]

Bicarbonates form via subsurface $CO_2$ incorporation (Reaction 1), and $Na^+$ from albite weathering (Equation F; Reaction 4). The low $Ca^{2+}$ (0.1196 meq/L) and high $SO_4^{2-}$ (10.5132 meq/L) suggest calcite precipitation. The alkaline, carbonate-rich setting ($CO_3^{2-}$ = 5.49 meq/L) favors this process (Appelo and Postma, 2005).

$Ca^{2+} + 2HCO_3^- \rightarrow CO_2 + H_2O + CaCO_3 \rightarrow \rightarrow$ *Reaction* [8]

This environment has also been reported in the Araró-Simirao geothermal zone (Pérez-Martínez, 2021).

### *5.3 Seasonal variation of electrical conductivity (EC) due to climatic factors*

Electrical conductivity (EC) measures the ability of water to conduct electric current (Freeze and Cherry, 1979), which depends on the concentration of dissolved ions. This parameter is useful for identifying seasonal changes in ion concentration in water (Garizi *et al.*, 2011).

In 2022, the aquifer's EC did not exhibit significant changes between seasons (Figure 8 A, B, C, D). However, in 2023, a seasonal variation in EC was observed between the rainy and dry seasons. This difference is attributed to the lower rainfall recorded in 2023 compared to 2022. While 796.73 mm of rainfall was recorded in 2022, only 547.9 mm fell in 2023 (SMN, 2025), a difference of 245.8 mm.

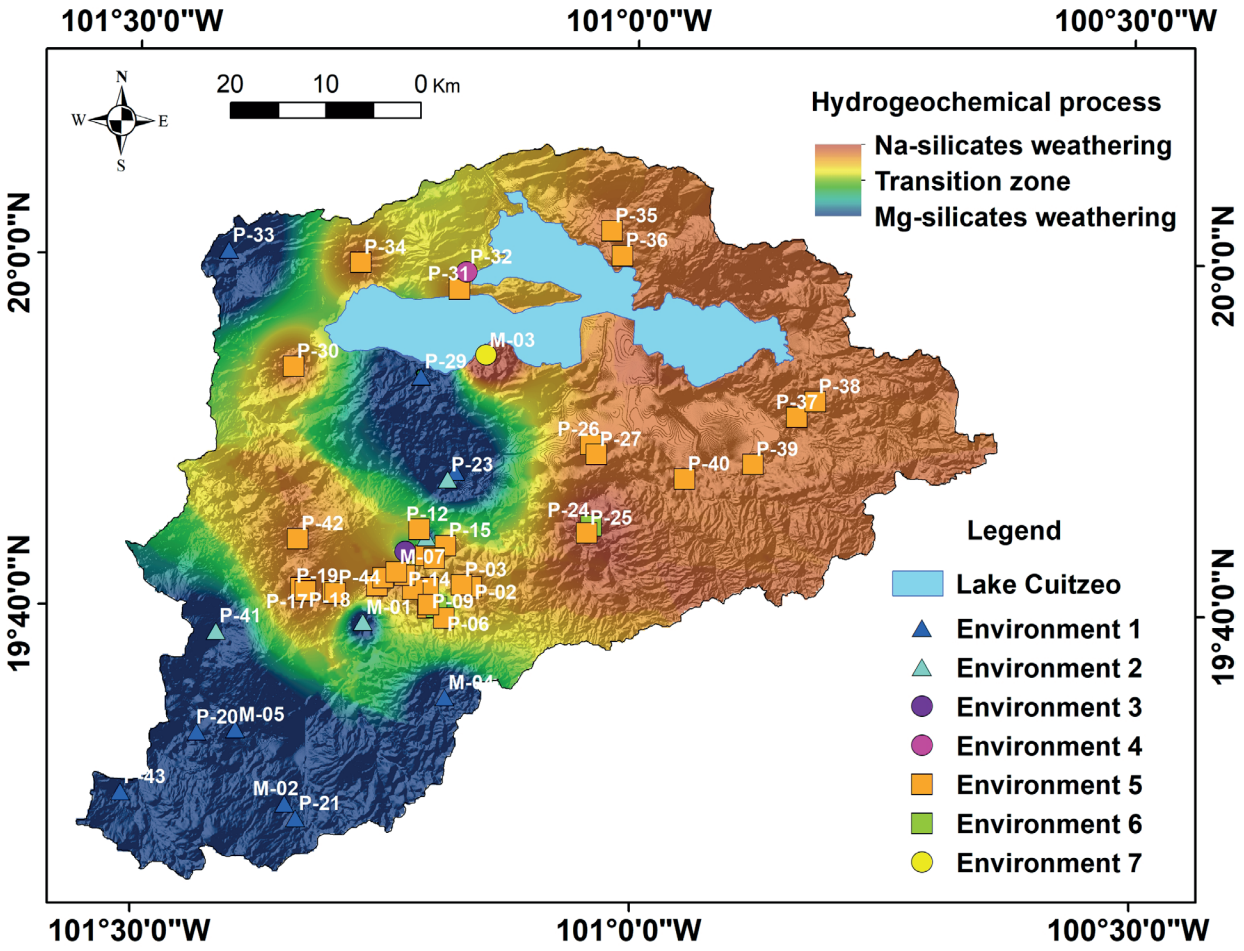


**Figure 7.** Hydrogeological environments obtained from the equations of D'Amore *et al.* (1983). The water-rock interaction allowed for the definition of seven environments: Environment 1, Mg-Ca waters and weathering of Mg-silicates; Environment 2, predominance of Mg-Na waters; Environment 3, weathering of plagioclases with ion exchange; Environment 4, calcareous carbonate with of Mg-silicate weathering; Environment 5, predominance of Na with weathering of Ca-Mg silicates and ion exchange; Environment 6, Ca-bicarbonate water and of Na-Mg silicate weathering; Environment 7, evaporitic with calcite precipitation. The background color gradient indicates the dominant hydrogeochemical process: Na-silicate weathering (orange), Mg-silicate weathering (blue), and a transitional zone between them (green).

The reduced rainfall in 2023 resulted in less water infiltrating the aquifer, thereby decreasing the dilution of dissolved salts in the groundwater. As a result, the salts became more concentrated, increasing the EC. Conversely, in 2022, higher rainfall allowed for better dilution of salts, maintaining lower EC values, as has been observed in other studies (Mahanta *et al.*, 2022).

Additionally, 2023 was 0.5 °C warmer than 2022 (SMN, 2025). This temperature difference caused an increase in evaporation by 24.36 mm during 2023 compared to the previous year (SMN, 2025). The higher evaporation rates in 2023 reduced the volume of subsurface water, further concentrating dissolved salts and consequently increasing the groundwater EC.

### *5.4 Groundwater flow systems and related hydrogeochemistry*

The three groundwater flow systems were identified using the Mifflin diagram (Figure 9). 82% of the water in the basin belongs to recent infiltration flow (41 sites), 16% to intermediate flow (8 sites), and 2% to deep circulation flow (one site). These flows occur within a heterogeneous and anisotropic unconfined aquifer, where localized semiconfined conditions are also present (CONAGUA, 2024b).

#### 5.4.1 Recent infiltration flow system

The recent infiltration flow system (Figure 10) moves southwest through the Michoacán-Guanajuato volcanic field and southward through the Mil Cumbres ignimbrites (Garduño-Monroy *et al.*, 2014). In the southeast and southwest, it transits the Atécuaro and La Escalera calderas, and the Indaparapeo and Garnica volcanic complexes (Figures 1 and 10). In the northwest, the water flows through andesitic lavas from the Leonera and

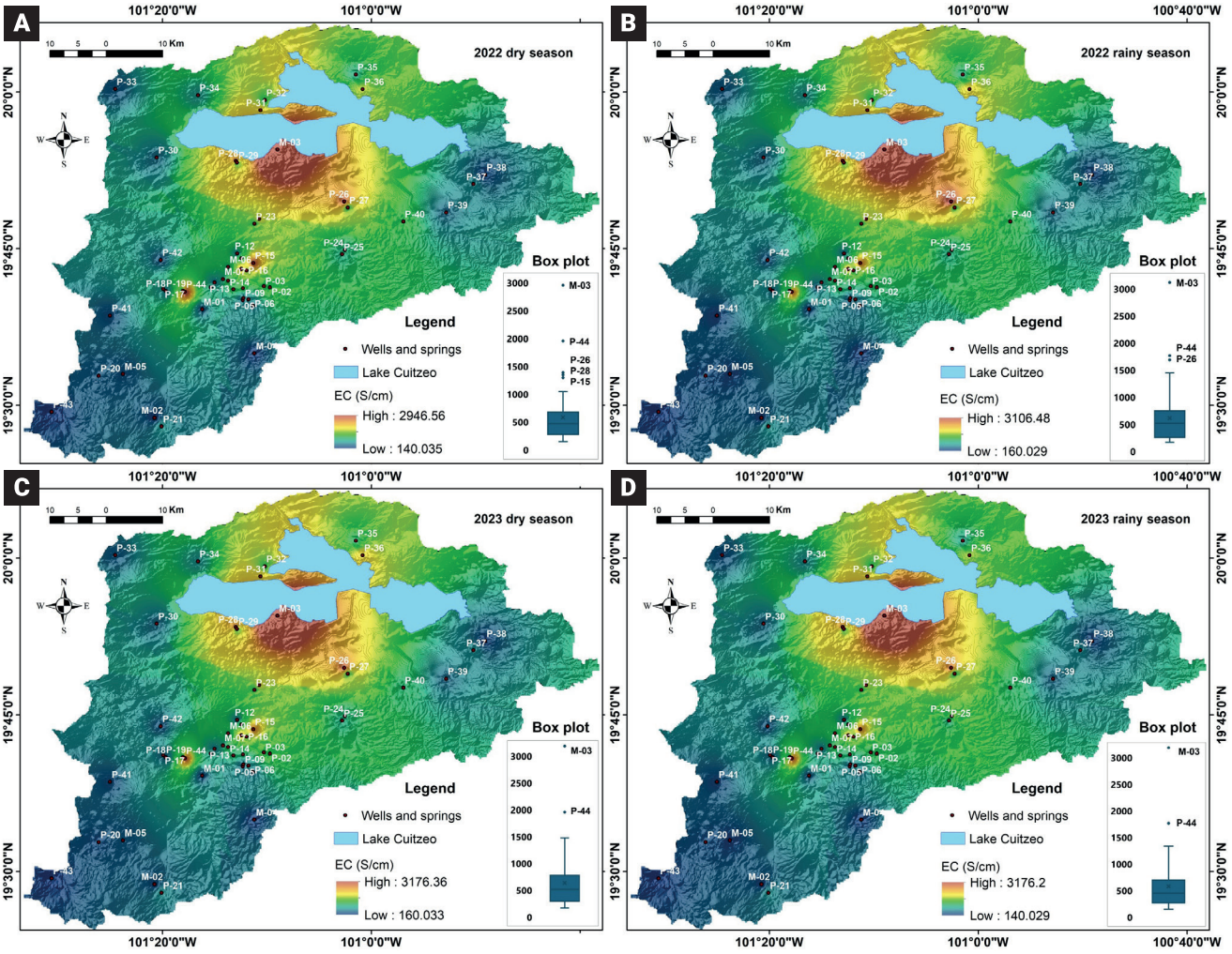


**Figure 8.** Electrical conductivity in A) Dry season 2022, B) Rainy season 2022, C) Dry season 2023, D) Rainy season 2023 in the Lake Cuitzeo basin. Data from the 51 sampled sites during each season were used.

Picacho stratovolcanoes and basalts from Sanabria and Villa Morelos (GSA, 1991), while in the northeast it passes through the Araró rhyolitic domes (GSA, 1991).

The temperature ranges from 15.9 to 32.2 °C (Figure 11), averaging 24 °C, higher than values reported for the southwestern sector, where ambient temperature is lower (Garduño-Monroy *et al.*, 2014; Pérez-Villarreal *et al.*, 2018), but consistent with other recent infiltration systems (Olea-Olea *et al.*, 2020).

Anomalously low temperatures (15.9 and 16.3 °C; Figure 11) were recorded at well P-43, located in Pátzcuaro, where average annual temperature is 17 °C and minimum 7.7 °C (Servicio Meteorológico Nacional, 2024a), both below the basin average (17.4 °C; CONAGUA, 2024b). In contrast, in the north, the average is 18.5 °C with minimums of 10.5 °C (Servicio Meteorológico Nacional, 2024b).

The temperature values are influenced by basin morphology; elevations in this area reach 3,426 m a.s.l. The highest value (32.2 °C) was recorded at well P-12 in Morelia, where intense groundwater extraction has caused cones of depression up to 150 m, limiting cold water recharge during the rainy season (Garduño-Monroy *et al.*, 2014).

Electrical conductivity (EC) ranges from 140 to 990 µS/cm, within potable limits (EC < 2500 µS/cm). Ion concentrations vary from 2.66 to 19.32 meq/L, consistent with recent infiltration flow (Toth, 1963). The pH ranges from 6.3 to 8.8. The lowest values (6.3 and 6.38) occur at wells P-21 and P-06, located in the fluvio-lacustrine sequence in the southwest. These slightly acidic pH values are attributed to meteoric water enriched in atmospheric $CO_2$, which forms carbonic acid ($H_2CO_3$) and releases $H^+$ ions (Freeze and Cherry, 1979).

$$CO_{2(g)}+H_2O_{(l)}\leftrightarrow H_2CO_{3(l)}\leftrightarrow HCO^-_{3(l)}+H_3O^+\rightarrow\rightarrow \textit{Reaction}\ [9]$$

More acidic pH values are observed in the south, where

rainfall is higher (801–1000 mm/year) than in the north (601–800 mm/year) (CONAGUA, 2024c).

Despite being recent infiltration, well P-33 in the northwest exhibits alkaline pH (8.8), likely due to natural neutralizing components in rainwater (Cano *et al.*, 2018) and the presence of calcite at equilibrium (SI=0.3). Calcite dissolution releases $Ca^{2+}$ and $HCO_3^-$ ions, increasing alkalinity (Appelo and Postma, 2005). Additional alkalinization may result from $NH_4^+$, $Ca^{2+}$, and $Mg^{2+}$ from agricultural activities (Zeng *et al.*, 2020).

All hydrogeological environments identified in the D'Amore diagram (1983) are present in this flow system, except the evaporitic environment with calcite precipitation. Main hydrogeochemical processes include weathering of Mg-Ca-Na silicates (e.g., olivine, albite, anorthite; Figure 4) and ion exchange.

Geological faults influence flow patterns (Bense *et al.*, 2013). Twenty-one faults have been identified in the basin, with dominant NW-SE, SW-NE, and recent E-W orientations (Garduño-Monroy *et al.*, 1999). These faults, along with the fractured and porous volcanic substrate, facilitate infiltration and transport of chemical species to lower basin sectors (Figure 10) following topography (Pérez-Villareal *et al.*, 2018).

#### 5.4.2 Intermediate flow system

Nearly 90% of the intermediate flow has been identified in the fluvio-lacustrine sequence (alluvium) at the basin center (Morelia), and along the northern and southern shores of Lake Cuitzeo (Figure 10). This system underlies the recent infiltration flow and is characterized by higher EC, temperature, and salinity (Tóth, 1963; 1999).

Temperatures range from 17.7 to 39.3 °C (Figure 11), higher than those of the recent infiltration flow and other intermediate systems in Mexico (Cardona and Carrillo-Rivera, 2006; Olea-Olea *et al.*, 2020), but similar to values previously reported in the basin's southwest (Pérez-Villarreal *et al.*, 2018). The highest temperature (39.2 °C) is observed at well P-44 in the southwest, where flow shows characteristics closer to deep circulation (Figure 9).

EC values range from 460 to 1950 µS/cm, all within potable limits (EC < 2500 µS/cm), and higher than those reported in other Mexican regions for similar flows (200 µS/cm; Cardona and Carrillo-Rivera, 2006). Ion concentrations range from 8.92 to 40.01 meq/L, exceeding those of recent infiltration (Figure 11).

The pH ranges from 6.7 to 7.9, generally indicating a balanced environment between $H^+$ and $OH^-$ ions, with a slight alkaline tendency. Hydrogeochemical processes in this system involve the weathering of Na-Ca silicates, mainly albite and, to a lesser extent, anorthite. At well P-01, calcite is supersaturated (SI=0.92), slightly increasing alkalinity (Figure 4).

The intermediate flow moves through SW-NE faults until it reaches the Tzitzio-Valle de Santiago Fault (T-VSF), intersected by E-W faults (Garduño-Monroy *et al.*, 2009). In the northern basin, E-W fault systems and the T-VSF control the intermediate groundwater flow (Figure 10).

#### 5.4.3 Deep circulation flow system

This system was identified in the fluvio-lacustrine sequence of the basin, specifically in the central sector of the southern shore of Lake Cuitzeo, in San Agustín del Maíz (Figures 1 and 10). It is characterized by higher EC, temperature, and salinity compared to local and intermediate flows (Tóth, 1963; 1999).

Represented by a single site (M-03), its characterization relies on the seasonal behavior of this thermal spring. The system presents the highest temperature of the three, with an average of 49 °C. Discharge temperatures in the area can reach up to 89 °C (Segovia *et al.*, 2005).

EC exceeds 3000 µS/cm, classifying the water as brackish (EC > 2500 µS/cm) (Pérez-Martínez *et al.*, 2021), surpassing values in the other two systems and nearby areas (Alfaro *et al.*, 2002). Brackish water is also present in the Araró-Simirao geothermal zone, where EC can reach 5900 µS/cm (Pérez-Martínez *et al.*, 2021). Ion concentration is the highest among all systems (60.31 meq/L), with notably low $Mg^{2+}$ content (0.0439 meq/L), typical of geothermal waters (Case *et al.*, 2011). The high mineralization is of igneous origin, resulting from water–mineral reactions at high temperature and pressure that dissolve ions ($Na^+$, $Ca^{2+}$, $SO_4^{2-}$, $Cl^-$), which reach the surface through faults (Li *et al.*, 2020).

The average pH is 9.0, higher than in the other systems and the basin average (pH = 7.4). Alkaline values in the northern sector had been previously reported (Alfaro *et al.*, 2002; Segovia *et al.*, 2005). This alkalinity results from the carbonation process and calcite precipitation.

Deep fluids ascend along faults, often depositing silica sinter, which is present in this area (Olvera-García *et al.*, 2020a). The sulfate facies suggests deeper flow than the bicarbonate facies (Chebotarev, 1955), indicating mixing from various depths, as observed in other geothermal systems (Brahim *et al.*, 2014). The thermal springs of San Agustín del Maíz are controlled by NNW- and WSW-trending fractures (Olvera-García, 2020b).

### *5.5 Vulnerability of local flows in the basin*

In Mexico, the agricultural sector exerts great pressure on water demand (Roy *et al.*, 2021), with 72% of the extracted groundwater being used for irrigation (UN, 2022). Of the three groundwater flow systems (Toth, 1963; 1999), the most susceptible to anthropogenic contamination is the recent infiltration flow

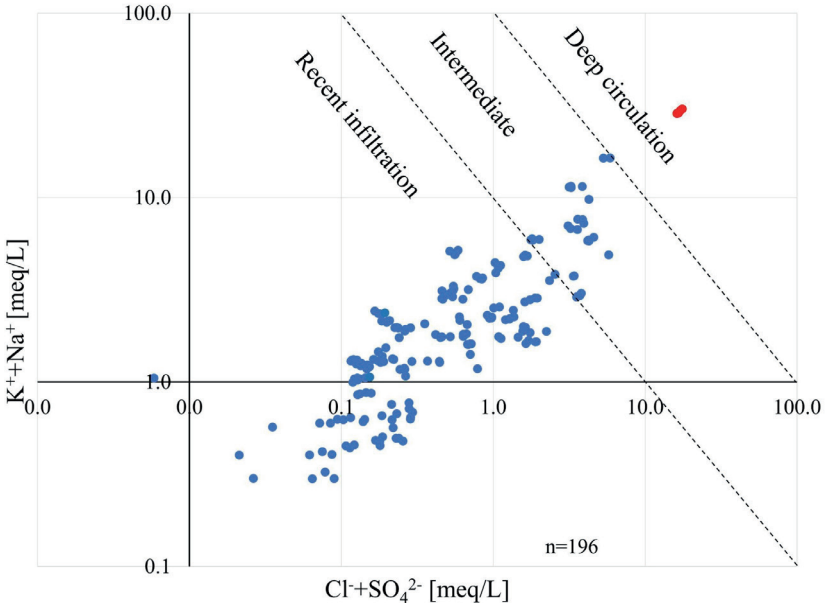


**Figure 9.** Classification of the groundwater flow systems in the Lake Cuitzeo basin based on the Mifflin diagram (1988). The blue color refers to cold water, and the red color to thermal water (49 °C) corresponding to the M-03 spring. Site P-44, classified as an intermediate system, shows a tendency towards deep circulation.

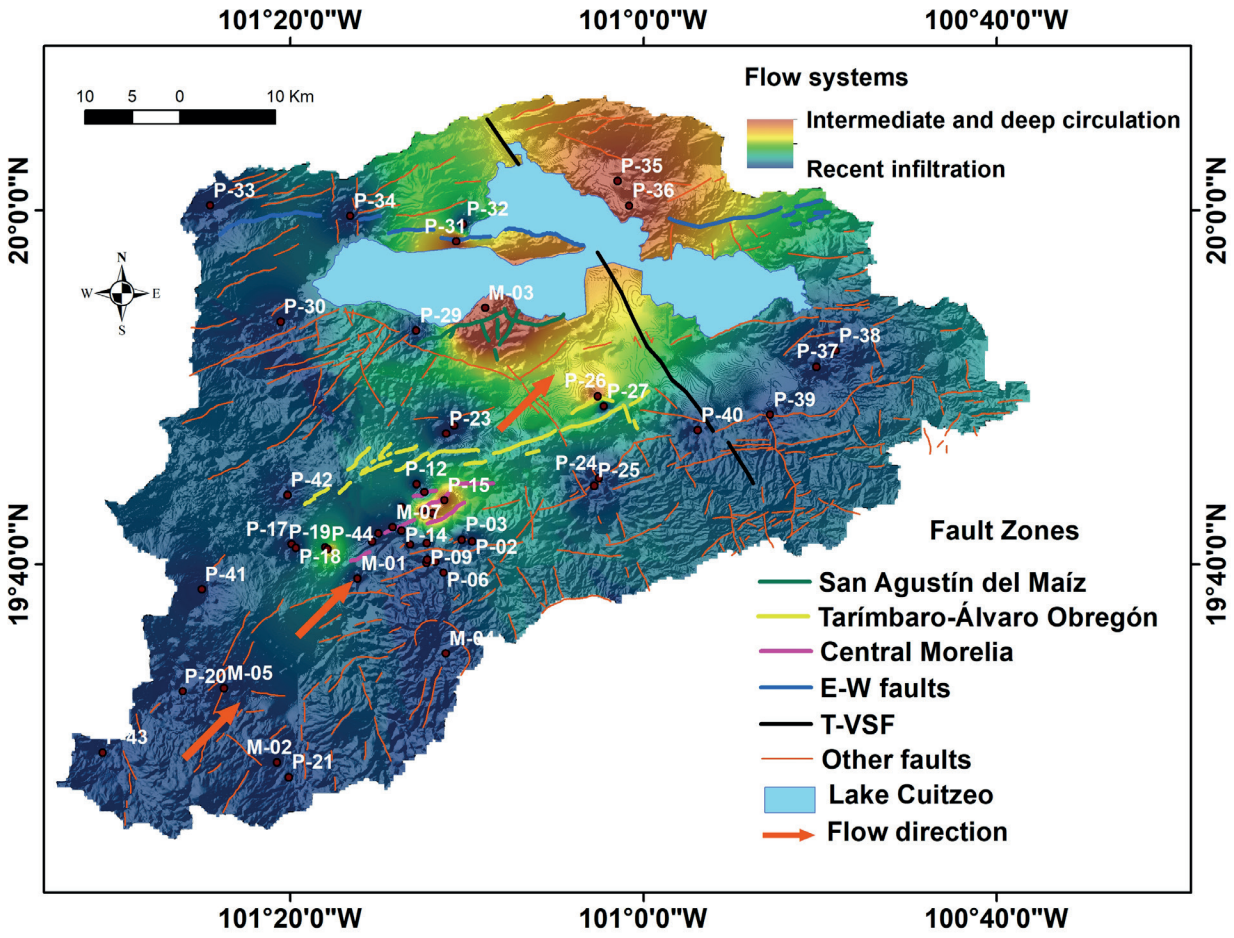


**Figure 10.** Distribution of flow systems based on hydrogeochemistry and their relationship with the fault systems in the basin. The flow direction of the basin is SW-NE (Garduño-Monroy *et al.*, 2014). The intermediate flow system and deep circulation are controlled by NW-SE faults in the center and E-W in the north, while the recent infiltration flows are associated with the E-W fault system present in the study area.

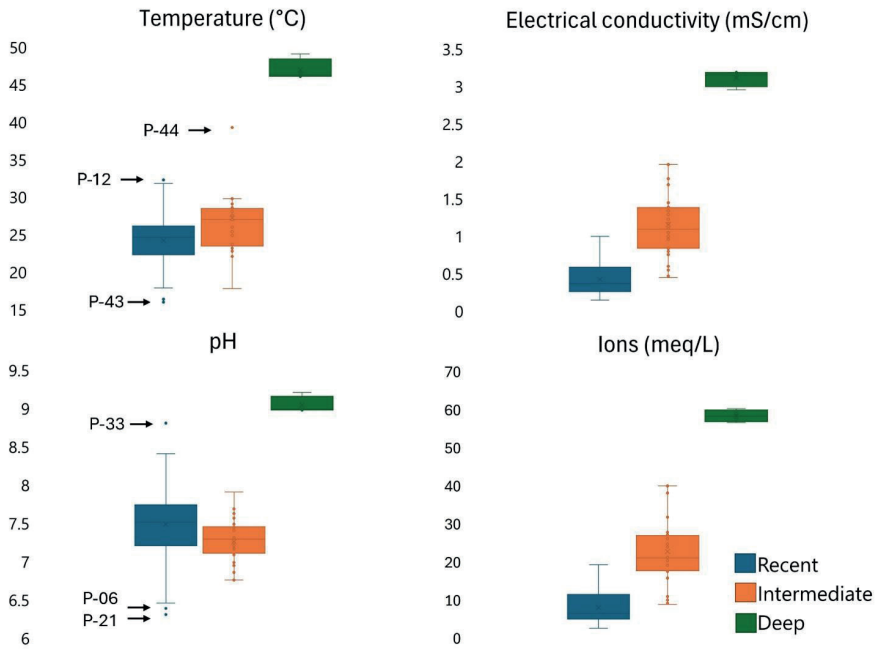


**Figure 11.** Physicochemical parameters of the flow systems in the Lake Cuitzeo basin represented in box plots. The colors indicate the flow system. The bars outside the box represent variability outside the upper and lower quartiles. The upper bar indicates the maximum value within 1.5 times the interquartile range above the third quartile. The lower bar shows the minimum value within 1.5 times the interquartile range below the first quartile. Outliers are found outside these bars and have their identifiers labeled.

due to its short travel through the subsurface (Burri *et al.*, 2019). In shallow flows, impacts on water chemistry related to irrigation returns (Burri *et al.*, 2019) and the application of fertilizers in agricultural areas (Burri *et al.*, 2019) have been identified. In the center of the basin, in recent infiltration flows, lies the 020 Morelia-Queréndaro irrigation district (CONAGUA, 2024b), an agricultural area where the use of fertilizers in agricultural practices threatens the water quality of these shallow flows. Over 1 million people live in the basin, where 40.21% of water use is for urban purposes (CONAGUA, 2024b).

According to the classification of the flow system in the basin, 82% of the water in the basin is recent infiltration flow, water that is vulnerable to contamination from various anthropogenic activities such as agricultural practices. Agriculture is the main factor of groundwater contamination (FAO, 2018).

### *5.6 Subsidence and groundwater extraction*

Subsidence is a gradual settling or sudden sinking of the ground surface due to the consolidation of sediments and, therefore, the movement of earth materials caused by stress (Galloway and Burbey, 2011). Subsidence, coupled with the Creep-Fault effect (slow and continuous deformation of lacustrine and fluvio-lacustrine sediments where geological faults control sediment deposition), poses a greater hazard due to its relationship along geological faults often obscured by anthropogenic activities (residential areas or farmlands). Creep-Fault subsidence is a global geological hazard (Bagheri-Gavkosh *et al.*, 2021).

76.92% of subsidence cases worldwide are due to anthropogenic activities, and 59.75% of these cases are due to water extraction (Bagheri-Gavkosh *et al.*, 2021). Strong correlations have also been observed between the subsidence rate and water extraction ($R^2 = 0.950$) with the decline of piezometric levels ($R^2 = 0.888$) (Bagheri-Gavkosh *et al.*, 2021).

The cities most affected by subsidence caused by water extraction are Beijing, Shanghai, Murcia, Bologna, Tokyo, Las Vegas, and Mexico City (Figueroa-Miranda *et al.*, 2018). Some of these regions are productive agricultural areas and/or overpopulated cities, where the demand for water for construction and domestic use generates subsidence (Bagheri-Gavkosh *et al.*, 2021).

In Mexico, intensive pumping has negatively impacted piezometric levels of aquifers in different cities experiencing subsidence, forming cones of depression of 180 m in Aguascalientes, 170 m in Morelia, 100 m in Celaya, 70 m in Salamanca, and 50 m in San Luis Potosí (Figueroa-Miranda *et al.*, 2018). Among the most affected urban areas is the city of Morelia, located in the center of the Lake Cuitzeo basin, which is home to over one million people. This city stands out due to both its demographic importance and the severity of ground deformation. Subsidence in Morelia reveals structurally-controlled ground motion at rates of up to −9 cm/year during 2014–2021 (Cigna and Tapete, 2022).

This phenomenon is most evident in the northwestern sector

of Morelia (Figueroa-Miranda *et al.*, 2020), where the highest subsidence rates, exceeding 100 meters have ben recorded in some areas (Pérez-Villarreal *et al.*, 2018). This zone corresponds to an area where lava flows from the Quinceo and Las Tetillas volcanoes overlie terrigenous lacustrine and fluvio-lacustrine sequences (Garduño-Monroy *et al.*, 2010), which are highly susceptible to compaction due to groundwater extraction, leading to surface deformation. This is the same area where the intermediate flows classified in this work and in those by Pérez-Villarreal *et al.* (2018, 2019) are located. Therefore, it is suggested that the previously reported subsidence is related to the extraction of water from intermediate flow systems that transit lacustrine and/or fluvio-lacustrine sediment sequences.

Continuing high water extraction from recent infiltration flow systems, as has been the case in northern Morelia, will generate subsidence processes, as already reported. On the other hand, water extraction from intermediate systems will aggravate subsidence in affected areas, creating geological hazards for the population.

### *5.7 Conceptual model of the Lake Cuitzeo basin based on water-rock interaction (Hydrogeochemistry)*

Several studies have classified the hydrogeochemical characteristics of water using various diagrams (Wang *et al.*, 2015; Zainol *et al.*, 2021; Islam *et al.*, 2022). To develop the hydrogeochemical conceptual model of the Lake Cuitzeo basin, D'Amore (1983), Mifflin (1988), and Piper (1954) diagrams were used, alongside Toth's flow system classification (1999), mineral saturation indices (Figure 4), piezometric data, and the direction of the geological fault systems in the basin (Garduño-Monroy *et al.*, 2014).

Groundwater flow in the basin begins in the southwest, where the Michoacán-Guanajuato Volcanic Field (MGVF), the El Águila semi-shield volcanism, and the Atécuaro Caldera are located (Figure 1). This flow corresponds to recent infiltration (Figure 10), characterized by cold temperatures (19.1 °C), low electrical conductivity (EC: 220 µS/cm), and neutral pH (7.1), the lowest recorded values in the basin for these parameters. The main hydrogeochemical processes in this region include olivine (Reaction 3) and anorthite (Reaction 2) weathering, as well as ion exchange, resulting in calcium and magnesium-rich waters. The sites in this zone include M-02, M-04, M-05, P-20, P-21, and P-43. The combination of shallow static water levels (Figure 2), recent infiltration flows (Figure 10), high precipitation, and significant elevations makes this region one of the basin's most important recharge areas. However, it also makes it one of the most vulnerable to anthropogenic contamination. Groundwater flows in a SW-NE direction (Garduño-Monroy *et al.*, 2014), guided by the geological fault system, until it reaches the basin center, dominated by a fluviolacustrine sequence (alluvium).

In the central basin, three groundwater flow systems were identified (Figure 10), where various hydrogeochemical processes occur, including Na-Ca-Mg silicate weathering, ion exchange, mixing of bicarbonate and sulfate waters, thermal activity, calcite precipitation, and gypsum dissolution. The water in this area shows average temperatures of 25.4 °C, a slightly alkaline pH (7.4), and higher EC (700 µS/cm) compared to the southwest. The sites included in this sector are P-01 to P-17, P-22, P-23, P-26, P-29, M-01, M-03, M-06, and M-07. Intermediate flow systems, guided by the SW-NE faults (central Morelia and Tarímbaro-Álvaro Obregón faults, Figure 10), direct water to the T-VSF fault, which ultimately transports the flow to the discharge area: Lake Cuitzeo (Garduño-Monroy *et al.*, 2004). The basin center has experienced the most significant groundwater drawdowns and land subsidence due to groundwater extraction.

In the southeast of the basin lie the Mil Cumbres Ignimbrites (IMC), the Araró Domes (DA), the Alegría Pumice Fall, and lahars (CPL) (Figure 1). These elevations generate recent infiltration flows (Figure 10) dominated by albite and anorthite weathering (Reactions 2 and 4) with ion exchange. These waters exhibit warm temperatures (26.3 °C), slightly alkaline pH (7.5), and moderate EC (460 µS/cm), lower than in the basin center. The sites in this region include P-24, P-25, P-27, P-37, P-38, P-39, and P-40. The Araró-Simirao geothermal field is located in this area, where NNW-SSE and NNE-SSW geological faults influence local geothermal manifestations (Pérez-Martínez *et al.*, 2021). Near the geothermal field (Zinapécuaro), sites such as P-38 have recorded underground temperatures of up to 31.1 °C. Groundwater flow in this area follows an E-W and SW-NW pattern toward the basin center and Lake Cuitzeo.

In the northern basin, intermediate flows predominate, exhibiting the highest recorded EC (790 µS/cm), slightly alkaline pH (7.4), and warm temperatures (26.4 °C). In this region, plagioclase weathering (Reactions 2 and 4) produces predominantly sodium-rich waters. Flows originate from the Manuna semi-shield volcanism, Cuitzeo lavas (LC), San Andrés lavas (LSA), and the San Andrés diorite (DSA) (Figure 1). The sites in this sector include P-35, P-36, P-32, and P-31. Subsurface flow is controlled by E-W faults and the Tzitio-Valle de Santiago fault, which direct water toward Lake Cuitzeo (Figure 10).

The western basin is characterized by recent infiltration flow systems, where the main hydrogeochemical processes include albite weathering and ion exchange. The flow passes through the Picacho stratovolcano, Las Tetillas, the fluviolacustrine sequence, and the MGVF (Figure 1), generating warm waters (26.7 °C), slightly alkaline pH (7.7), and EC of 500 µS/cm. The sites in this sector are P-18, P-19, P-30, P-33, P-34, P-42, and P-44. SW-NE faults guide groundwater toward Lake Cuitzeo (Figure 10).

In summary, the spatial distribution and hydrochemical characterization of groundwater in the Lake Cuitzeo basin revealed that 82% of the water corresponds to recent infiltration flow, predominantly located in the southwest and western regions, and characterized by low salinity, neutral pH, and magnesium enrichment from silicate weathering. Intermediate flows (16%) are concentrated in the basin center and along the lake margins, where higher EC, temperatures, and sodium concentrations are observed, and where groundwater extraction has been linked to subsidence processes. Deep circulation flow (2%) was identified at a single thermal spring, exhibiting high salinity, elevated temperature, and mixed sulfate-bicarbonate composition. Seven hydrogeological environments were recognized based on the dominant cation, lithological composition, and hydrochemical processes. The integration of geochemical modeling, flow system classification, and structural geology provides a robust conceptual framework that improves the understanding of water-rock interaction and flow dynamics in the basin. These findings are essential for identifying vulnerable areas, assessing the impact of extraction practices, and guiding sustainable water resource management.

## 6. Conclusions

This study provides an integrated understanding of groundwater flow systems and their associated hydrogeochemical processes in the Lake Cuitzeo basin. A total of 204 water samples collected in two years, were analyzed from wells and springs across the basin, allowing the identification of three groundwater flow systems: recent infiltration (82%), intermediate (16%), and deep circulation (2%), and the classification of seven distinct hydrogeological environments.

The chemical composition of groundwater reflects dominant water–rock interaction processes, including the weathering of Ca-Na-Mg silicates, ion exchange with clays, $CO_2$ dissolution (carbonation), mixing of different water types, calcite precipitation, and gypsum dissolution. Sodium-bicarbonate (Na-$HCO_3$) waters were predominant (36.2%), with lesser proportions of magnesium and mixed cation types. Saturation indices and geochemical modeling confirmed the presence of silicate, carbonate, halide, and sulfate mineral phases.

The results highlight how groundwater quality and chemistry are shaped by lithological composition, tectonic structure (e.g., fault systems), and hydrological dynamics. Geological faults not only guide flow paths but also promote water mixing and mineral dissolution and precipitation.

This work contributes to a better understanding of groundwater-rock interaction in volcanic-tectonic basins, providing a hydrogeochemical conceptual model that identifies recharge areas, vulnerable zones, and the role of flow systems in water chemistry evolution. These insights are critical for sustainable groundwater management, particularly in the context of overextraction and land subsidence. In urban centers like Morelia with 849,053 inhabitants (INEGI, 2024), where intense extraction from intermediate flow systems has already triggered subsidence, strategic water use planning based on flow system vulnerability is essential to ensure long-term water availability and reduce geological risk.

## 7. Acknowledgments

The authors thank the staff of the Organismo Operador de Agua Potable, Alcantarillado y Saneamiento de Morelia (OOAPAS) for their support during the sampling of wells and springs. Special thanks to biologist Luis Erick Arroyo Sesento, analytical technician at the Instituto de Geofísica, Unidad Michoacán (IGUM, UNAM), for his collaboration in sample processing. We also acknowledge the Geochemical Laboratory for Geothermal Fluids at IGUM, UNAM, for their assistance with the chemical analysis of water samples. Financial support was provided by the Secretaría de Ciencia, Humanidades, Tecnología e Innovación (Secihti) through a doctoral scholarship, and academic support by the Institutional Doctoral Program in Biological Sciences at the Universidad Michoacana de San Nicolás de Hidalgo (UMSNH). We extend our sincere gratitude to Dr. José Alfredo Ramos Leal for his valuable comments that enriched the manuscript, and to the anonymous reviewer for constructive feedback and suggestions.

## 8. References

Alfaro, R., Martínez, V., Segovia, N., Peña, P., López, M., Armienta, M., Rangel, J., Seidel, J. (2002). Radon behavior in springs and wells around Cuitzeo lake, Lerma river basin, Mexico. *Geofísica Internacional*, 41(4), 439-445. doi: **https://doi.org/10.22201/igeof.00167169p.2002.41.4.492**

Amézaga-Campos, B. S., Villanueva-Estrada, R., Carrillo-Chavez, A., Morales-Arredondo, J. I., & Morán-Ramírez, J. (2022). Hydrogeochemistry characterization of an overexploited municipal, agricultural, and industrial aquifer, central Mexico. Applied Geochemistry, 142, 105310. doi: **https://doi.org/10.1016/j.apgeochem.2022.105310**

Appelo, C., & Postma, D. (2005). *Geochemistry, groundwater and pollution* (2a ed.). Amsterdam: A. A. Balkema Publishers.

Avellán, D. R., Cisneros-Máximo, G., Macías, J. L., Gómez-Vasconcelos, M. G., Layer, P. W., Sosa-Ceballos, G., & Robles-Camacho, J. (2020). Eruptive chronology of monogenetic volcanoes northwestern of Morelia – Insights into volcano-tectonic interactions in the central-eastern

Michoacán-Guanajuato Volcanic Field, México. *Journal of South American Earth Sciences*, 100, 102554. doi: **https://doi.org/10.1016/j.jsames.2020.102554**

Bagheri-Gavkosh, M., Hosseini, S. M., Ataie-Ashtiani, B., Sohani, Y., Ebrahimian, H., Morovat, F., & Ashrafi, S. (2021). Land subsidence: A global challenge. *Science of the Total Environment*, 778, 146193. doi: **https://doi.org/10.1016/j.scitotenv.2021.146193**

Beck, H. E., Zimmermann, N. E., McVicar, T. R., Vergopolan, N., Berg, A., & Wood, E. F. (2018). Present and future Köppen-Geiger climate classification maps at 1-km resolution. *Scientific Data*, 5, 180214. doi: **https://doi.org/10.1038/sdata.2018.214**

Bense, V., Gleeson, T., Loveless, S., Bour, O., & Scibek, J. (2013). Fault zone hydrogeology. *Earth-Science Reviews*, 127, 171-192. doi: **https://doi.org/10.1016/j.earscirev.2013.09.008**

Brahim, F. B., Makni, J., Bouri, S., & Dhia, H. B. (2014). Evaluation of Temperature and Mixing Process of Water in Deep and Shallow Aquifers in the Southwestern Tunisia: Case of Djerid Region. *Arabian Journal of Science and Engineering*, 39, 5677-5689. doi: **https://doi.org/10.1007/s13369-014-1138-z**

Burri, N. M., Weatherl, R., Moeck, C., & Schirmer, M. (2019). A review of threats to groundwater quality in the anthropocene. *Science of The Total Environment*, 684, 136-154. doi: **https://doi.org/10.1016/j.scitotenv.2019.05.236**

Cano, Y., Sánchez, L., Puentes, J. T., & Velásquez, M. L. (2018). Evaluación preliminar del pH de las lluvias en la ciudad de Portoviejo, Ecuador. *Ciencia*, 26(3-4), 79-83. doi: **https://doi.org/10.5281/zenodo.5590926**

Cardona, A., & Carrillo-Rivera, J. J. (2006). Hidrogeoquímica de sistemas de flujo intermedio que circulan por sedimentos continentales derivados de rocas riolíticas. *Ingeniería Hidráulica en México*, 21(3), 69-86.

Cardona-Melchor, S. (2015). Estudio vulcanológico del Complejo Volcánico El Águila y los domos La Taza-La Nieve-El burro centro-norte de Michoacán. [*Master thesis*.] *Instituto de Investigaciones en Ciencias de la Tierra, UMSNH, Morelia, México.*

Case, D. H., Wang, F., & Giammar, D. E. (2011). Precipitation of Magnesium Carbonates as a Function of Temperature, Solution Composition, and Presence of a Silicate Mineral Substrate. Environmental Engineering Science, 28(12), 881-889. doi: **https://doi.org/10.1089/ees.2010.0341**

Chebotarev, I. (1955). Metamorphism of Natural Waters in the Crust of Weathering-1. *Geochimica et Cosmochimica Acta*, 8(1-2), 22-48. doi: **https://doi.org/10.1016/0016-7037(55)90015-6**

Chihi, H., Marsily, G. D., Belayouni, H., & Yahyaoui, H. (2015). Relationship between tectonic structures and hydrogeochemical compartmentalization in aquifers: Example of the "Jeffara de Medenine" system, south–east Tunisia. *Journal of Hydrology: Regional Studies*, 4(B), 410-430. doi: **https://doi.org/10.1016/j.ejrh.2015.07.004**

Cigna, F., & Tapete, D. (2022). Urban growth and land subsidence: Multi-decadal investigation using human settlement data and satellite InSAR in Morelia, Mexico. Science of The Total Environment, 811, 152211. doi: **https://doi.org/10.1016/j.scitotenv.2021.152211**

CONAGUA. (2007). Actualización de la disponibilidad media anual de agua en el acuífero Morelia-Queréndaro (1602), Estado de Michoacán. Comision Nacional del Agua.

CONAGUA. (2020). Actuaización de la disponibilidad media anual de agua en el acuífero Morelia-Queréndaro (1602), Estado de Michoacán. Comision Nacional del Agua.

CONAGUA. (2024a). *Sistema Nacional de Información del Agua SINA 3.0.* Recuperdo el 24 de julio de 2024 de **https://sinav30.conagua.gob.mx:8080/SINA/?opcion=acuiferos**

CONAGUA. (2024b). *Actualización de la disponibilidad media anual de agua en el acuifero Morelia-Queréndaro (1602), Estado de Michoacán.* Comision Nacional del Agua.

CONAGUA. (2024c). *Sistema Nacional de Información del Agua SINA 3.0.* Recuperado el 25 de julio de 2024 de **https://sinav30.conagua.gob.mx:8080/SINA/?opcion=precipitacion**

D'Amore, F., Scandiffio, G., & Panichi, C. (1983). Some observations in the chemical classification of ground waters. *Geothermics*, 12(2-3), 141-148. doi: **https://doi.org/10.1016/0375-6505(83)90024-X**

Das, P., Mohapatra, P., Goswami, S., Mishra, M., & Pattanaik, J. (2020). A geospatial investigation of interlinkage between basement fault architecture and coastal aquifer hydrogeochemistry. *Geoscience Frontiers*, 11(4), 1431-1440. doi: **https://doi.org/10.1016/j.gsf.2019.12.008**

Drever, J. I. (1997). The geochemistry of natural waters surface and groundwater environments (3a ed.). New Jersey: Prentice-Hall Inc.

Esri. (2024). ArcGis Pro. Recuperado el 29 de mayo de 2024 de **https://pro.arcgis.com/es/pro-app/latest/help/analysis/geostatistical-analyst/how-inverse-distance-weighted-interpolation-works.htm**

FAO. (2018). *More people, more food, worse water? a global review of water pollution from agriculture*. Recuperado el 25 de julio de 2018 de Food and Agriculture Organization of the United Nations: **http://www.fao.org/3/CA0146EN/ca0146en.pdf**

Figueroa-Miranda, S., Hernández-Madrigal, V. M., Tuxpan-Vargas, J., & Villaseñor-Reyes, C. I. (2020). Evolution assessment of Structurally-Controlled Differential Subsidence using SBAS and PS Interferometry in an emblematic case of central Mexico. *Engineering Geology*, 279, 105860. doi: **https://doi.org/10.1016/j.enggeo.2020.105860**

Figueroa-Miranda, S., Tuxpan-Vargas, J., Ramos-Leal, J. A., Hernández-Madrigal, V. M., & Villaseñor-Reyes, C. I. (2018). Land subsidence by groundwater over-exploitation from aquifers in tectonic valleys of Central México: A review. *Engineering Geology*, 246, 91-106. doi: **https://doi.org/10.1016/j.enggeo.2018.09.023**

Freeze, R. A., & Cherry, J. A. (1979). *Groundwater.* New Jersey: Prentice-Hall.

Galloway, D. L., & Burbey, T. J. (2011). Review: Regional land subsidence accompanying groundwater extraction. *Hydrogeology Journal*, 19, 1459–1486. doi: **https://doi.org/10.1007/s10040-011-0775-5**

Garduño-Monroy, V. H., Giordano, N., Olivera, J. A., Madrigal, V. M.,

Nateras, A. S., & Salmerón, J. E. (2014). Estudio hidrogeológico del sistema acuífero de Morelia, Michoacán, para una correcta planificación del territorio. In A. Vieyra, & A. Larrazábal. (Eds), *Urbanización, Sociedad y Ambiente. Experiencias en ciudadades medias* (pp. 193-218). Universidad Nacional Autónoma de México, Centro de investigaciones en Geografía Ambiental.

Garduño-Monroy, V. H., Medina-Vega, V. H., Israde-Alcántara, I., Hernández-Madrigal, V. M., & Ávila-Olivera, J. A. (2010). Unidades geohidrológicas de la region Morelia-Cuitzeo. En A. Cram, L. Galicia, & I. I.-A. (Eds), *Atlas de la cuenca del Lago de Cuitzeo: Análisis de su geografía y entorno socioambiental* (pp. 64-67). Universidad Nacional Autónoma de México, Instituto de Geografía; Universidad Michoacana de San Nicolás de Hidalgo.

Garduño-Monroy, V. H., Pérez-Lopez, R., Israde-Alcantara, I., Rodríguez-Pascua, M. A., Szynkaruk, E., Hernández-Madrigal, V. M., García-Zepeda, M. L., Corona-Chávez, P., Ostroumov, M., Medina-Vega, V. H., García-Estrada, G., Carranza, O., Lopez-Granados, E., Mora, J. C. (2009). Paleoseismology of the southwestern Morelia-Acambay fault system, central Mexico. *Geofísica Internacional*, 48(3), 319-355. doi: **https://doi.org/10.22201/igeof.00167169p.2009.48.3.29**

Garduño-Monroy, V. H., Rodríguez-Torres, G., Israde-Alcántara, I., Arreygue, E., Canuti, P., & Chiesa, S. (1999). Efecto del clima (El niño) en los fenómenos de fluencia de las fallas geológicas de la ciudad de Morelia. GEOS, 19(2), 84-93.

Garizi, A. Z., Sheikh, V., & Sadoddin, A. (2011). Assessment of seasonal variations of chemical characteristics in surface water using multivariate statistical methods . *International Journal of Environmental Science & Technology*, 8(3), 581, 592. doi: **https://doi.org/10.1007/BF03326244**

Geological Society of America (GSA). (1991). *Geologic map of the central sector of the Mexican volcanic belt, states of Guanajuato and Michoacan, Mexico.* Boulder, Colorado: Geological Society of America Map and Chart Series MCH-072.

Glynn, P. D., & Plummer, L. N. (2005). Geochemistry and the understanding of ground-water systems. *Hydrogeology Journal*, 13, 263-287. doi: **https://doi.org/10.1007/s10040-004-0429-y**

Gómez-Cruz, K. (2020). Estudio de la hidrogeoquímica y calidad del agua subterránea en la cuenca del Lago de Cuitzeo. [Master's thesis]. *Universidad Michoacana de San Nicolás de Hidalgo.*

Gómez-Moncada, R. A., Mora, A., Jaramillo, M., Parra, M., Mayorga, H., Martínez, A., Suárez,D., Sandoval-Muñoz, J., Sandoval-Ruiz, J., Caballero, V., Jiménez, M., Bueno, R., Saylor, J. E. (2022). Decoding of groundwater recharge in deep aquifers of foreland Basins using stable isotopes (δ18O and δD) and anion-cation analysis: A case study in the southern Llanos Basin, Colombia. *Journal of South American Earth Sciences*, 120, 104079. doi: **https://doi.org/10.1016/j.jsames.2022.104079**

Gómez-Vasconcelos, M., Avellán, D., Soria-Caballero, D., Macías, J., Velázquez-Bucio, M., Jiménez-Haro, A., Israde-Alcántara, I., Garduño-Monroy, V. H., Ávila-Olivera, J. A., Figueroa-Soto, Á. G., Cisneros-Máximo, G., Cardona-Melchor, S. (2021). Geomorphic characterization of faults as earthquake sources in the Cuitzeo Lake basin, central México. Journal of South American Earth Sciences, 109, 103196. doi: **https://doi.org/10.1016/j.jsames.2021.103196**

Gómez-Vasconcelos, M., Garduño-Monroy, V., Macías, J., Layer, P., & Bonowitz, J. (2015). The sierra de Mil Cumbres, Michoacán, Mexico: Transitional volcanism between the Sierra Madre Occidental and the Trans-Mexican Volcanic Belt. *Journal of Volcanology and Geothermal Research*, 301, 128-147. doi: **https://doi.org/10.1016/j.jvolgeores.2015.05.005**

Hartanto, P., Alam, B. Y., Lubis, R. F., Ismawan, I., Iskandarsyah, T. W., Sendjaja, Y. A., & Hendarmawan, H. (2022). The application of hydrogeochemical and stable isotope data to decipher the origin and evolution of hot springs in the Rawadanau Basin, Indonesia. *Geothermics*, 105, 102506. doi: **https://doi.org/10.1016/j.geothermics.2022.102506**

Hem, J. D. (1985). *Study and Interpretation of the Chemical Characteristics of Natural Water*. Alexandria, VA: U. S. G. S.

Hernández-Guzmán, R., Ruiz-Luna, A., & Mendoza, E. (2021). Sara4r: an R graphical user interface (GUI) to estimate watershed surface runoff applying the NRCS – curve number method. *Journal of Hydroinformatics*, 23(1), 76–87. doi: **https://doi.org/10.2166/hydro.2020.087**

Hounslow, A. W. (1995). *Water quality data: Analysis and interpretation*. CCR Press, Inc.

INEGI. (2024). *Censo de población y vivienda 2020, INEGI.* Recuperado el 24 de julio de 2025 de **https://www.inegi.org.mx/app/cpv/2020/resultadosrapidos/default.html?texto=Morelia**

Islam, M. S., & Mostafa, M. G. (2022). Evaluation of Hydrogeochemical Processes in Groundwater Using Geochemical and Geostatistical Approaches in the Upper Bengal Basin. *Geofluids*, 9591717, 1-21. doi: **https://doi.org/10.1155/2022/9591717**

Israde-Alcántara, I., & Garduño-Monroy, V. H. (1999). Lacustrine record in a volcanic intra-arc setting: the evolution of the Late Neogene Cuitzeo basin system (central-western Mexico, Michoacán). *Palaeogeography, Palaeoclimatology, Palaeoecology*, 151(1-3), 209–227. doi: **https://doi.org/10.1016/S0031-0182(99)00024-3**

Israde-Alcántara, I., Velázquez-Durán, R., García, M. S., James, Vázquez, G. D., & Garduño-Monroy, V. H. (2010). Paleolimnological evolution of Lake Cuitzeo, Michoacan during the Pleistocene-Holocene. *Boletín de la Sociedad Geológica Mexicana*, 62(3), 345-357. doi: **http://dx.doi.org/10.18268/BSGM2010v62n3a3**

Lewis, A. L., Sarkar, B., Wade, P., Kemp, S. J., Hodson, M. E., Taylor, L. L., . . . Beerlin, D. J. (2021). Effects of mineralogy, chemistry and physical properties of basalts on carbon capture potential and plant-nutrient element release via enhanced weathering. Applied Geochemistry, 132, 105023 doi: **https://doi.org/10.1016/j.apgeochem.2021.105023**

Li, C., Gao, X., Li, S., & Bundschuh, J. (2020). A review of the distribution, sources, genesis, and environmental concerns of salinity in groundwater. *Environmental Science and Pollution Research*, 27, 41157-41174. doi: **https://doi.org/10.1007/s11356-020-10354-6**

Mahanta, A. R., Rawat, K. S., Singh, S. K., Sanjeevi, S., & Mishra, A. K. (2022). Evaluation of long-term nitrate and electrical conductivity in groundwater system of Peninsula, India. *Applied Water Science*, 12(17). doi: **https://doi.org/10.1007/s13201-021-01568-1**

Mifflin, M. (1988). Region 5, Great Basin. En W. Back, J. S. Rosenshein, & P. R. Seaber (Eds), *Hydrogeology* (pp. 69-78). Geological Society of America. doi: https://doi.org/10.1130/DNAG-GNA-O2.69

Negrel, P., Pauwels, H., Dewandel, B., Gandolfi, J., Mascré, C., & Ahmed, S. (2011). Understanding groundwater systems and their functioning through the study of stable water isotopes in a hard-rock aquifer (Maheshwaram watershed, India). *Journal of Hydrology*, 397(1-2), 55-70. doi: **https://doi.org/10.1016/j.jhydrol.2010.11.033**

Norma Oficial Mexicana NOM-127-SSA1-2021, Agua para uso y consumo humano. Límites permisibles de la calidad del agua. (02 de mayo de 2022) **https://www.dof.gob.mx/nota_detalle.php?codigo=5650705&fecha=02/05/2022#gsc.tab=0**

Norma Oficial Mexicana NOM-230-SSA1-2002. Salud ambiental. Agua para uso y consumo humano, requisitos sanitarios que se deben cumplir en los sistemas de abastecimiento públicos y privados durante el manejo del agua. Procedimientos sanitarios para el muestreo. (17 de julio de 2025) **https://www.dof.gob.mx/nota_detalle.php?codigo=2081772&fecha=12/07/2005&print=true**

Olea-Olea, S., Escolero, O., Mahlknecht, J., Ortega, L., Taran, Y., Moran-Zenteno, D. J., Zamora-Martínez, O., Tadeo-Leon, J. (2020). Water-rock interaction and mixing processes of complex urban groundwater flow system subject to intensive exploitation: The case of Mexico City. *Journal of South American Earth Sciences*, 103, 102719. doi: **https://doi.org/10.1016/j.jsames.2020.102719**

Olvera-García, E., Garduño-Monroy, V. H., Ostrooumov, M., Bermejo-Santoyo, G., Guevara-Alday, J. A., Brogi, A., & Liotta, D. (2020a). Litofacies y mineralogía de los depósitos de sínter de la zona geotérmica de San Agustín del Maíz, Michoacán, México. *Revista Mexicana de Ciencias Geológicas*, 37(3), 212-223. doi: **https://doi.org/10.22201/cgeo.20072902e.2020.3.1585**

Olvera-García, E., Garduño-Monroy, V., Liotta, L., Brogi, A., Bermejo-Santoyo, G., & Guevara-Alday, J. (2020b). Neogene-Quaternary normal and transfer faults controlling deep-seated geothermal systems: The case of San Agustín del Maíz (central Trans-Mexican Volcanic Belt, México). *Geothermics*, 86, 101791. doi: **https://doi.org/10.1016/j.geothermics.2019.101791**

Pérez-Martínez, I., Villanueva-Estrada, R. E., García-Martínez, R., Rodríguez-Díaz, A., & Canet, C. (2021). Anomalías y mecanismos de transporte de mercurio en un sistema hidrotermal asociado a fallas normales en Araró, Michoacán (occidente de México). *Revista Mexicana de Ciencias Geológicas*, 38(2), 86-99. doi: **http://dx.doi.org/10.22201/cgeo.20072902e.2021.2.1596**

Pérez-Villarreal, J., Ávila-Olivera, J. A., & Israde-Alcántara, I. (2018). Análisis de los sistemas de flujo en un acuífero perturbado por la extracción de aguas subterráneas. Caso zona Morelia-Capula, Michoacán. *Boletín de la Sociedad Geológica Mexicana*, 70(3), 675-688. doi: **http://dx.doi.org/10.18268/BSGM2018v70n3a5**

Pérez-Villarreal, J., Ávila-Olivera, J. A., Israde-Alcántara, I., & Delgado, O. B. (2019). Nitrate as a parameter for differentiating groundwater flow systems in urban and agricultural areas: the case of Morelia-Capula area, Mexico. *Hydrogeology Journal*, 27, 1767-1778. doi: **https://doi.org/10.1007/s10040-019-01933-0**

Piper, A. (1944). A graphic procedure in the geochemical interpretation of water analyses. *EOS, Transactions American Geophysical Union*, 25(6), 914-928. doi: **http://dx.doi.org/10.1029/TR025i006p00914**

Ramos-Leal, J. A., Morán-Ramírez, J., Silva-García, J. T., Fuentes-Rivas, R. M., Cruz-Cárdenas, G., Ochoa-Estrada, S., & Estrada-Godoy, F. (2018). Identification of hydrogeochemical processes in a volcano-sedimentary aquifer of Ciénega de Chapala in Michoacán, Mexico. *Arabian Journal of Geosciences*, 11, 422. doi: **https://doi.org/10.1007/s12517-018-3760-7**

Roy, P. D., Selvam, S., Venkatramanan, S., Logesh, N., Lakshumanan, C., & Sánchez-Zavala, J. L. (2021). Identification of sources and groundwater recharge zones from hydrochemistry and stable isotopes of an agriculture-based paleo-lacustrine. *Geochemistry*, 81(2), 125742. doi: **https://doi.org/10.1016/j.chemer.2021.125742**

Segovia, N., Barragán, R. M., Alfaro, R., Arellano, V. M., & Mena, M. (2010). Fluid-Mineral Equilibrium of Spring Waters at Cuitzeo Basin (Mexico) Geothermal Zone. *Proceedings World Geothermal Congress 2010*, 1-7.

Segovia, N., Barragan, R. M., Tello, E., Alfaro, R., & Mena, M. (2005). Geochemical Characteristics and 222Rn Measurements at Cuitzeo Basin (Mexico) Thermal Springs and Artesian Wells. *Proceedings World Geothermal Congress 2005*, 1-6

Servicio Meteorológico Nacional. (2024a*). Normales Climatológicas. Estación: 16087.* Recuperado el 05 de abril 2024 de **https://smn.conagua.gob.mx/tools/RESOURCES/Normales5110/NORMAL16087.TXT**

Servicio Meteorológico Nacional. (2024b). *Normales climatológicas. Estación: 16027*. Recuperado el 05 de abril 2024 de **https://smn.conagua.gob.mx/tools/RESOURCES/Normales_Climatologicas/Normales8110/mich/nor8110_16027.txt**

Servicio Meteorológico Nacional. (2025). Normales climatológicas por Estado. Recuperado el 01 de enero 2025 de **https://smn.conagua.gob.mx/es/climatologia/informacion-climatologica/normales-climatologicas-por-estado?estado=mich**

Tóth, J. (1963). A Theoretical Analysis of Groundwater Flow in Small Drainage Basins. *Journal of Geophysical Research*, 68(16), 4795-4812. doi: **https://doi.org/10.1029/JZ068i016p04795**

Toth, J. (1999). Groundwater as a geologic agent: An overview of the causes, processes, and manifestations. *Hydrogeology Journal*, 7, 1-14. doi: **https://doi.org/10.1007/s100400050176**

Trujillo-Hernández N, Garduño-Monroy V. H., Jiménez-Haro A, Gómez-Álvarez F, Nájera-Blas S. M., Israde-Alcántara I., Layer P. (2022).

Estratigrafía volcánica de la porción suroeste del Lago de Cuitzeo y su relación con la formación de la caldera tipo graben de Chucándiro. Revista Mexicana de Ciencias Geológicas, 39(1),100–115. doi: **https://doi.org/10.22201/cgeo.20072902e.2022.1.1689**

UNESCO. (2022). *The United Nations World Water Development Report 2022: Groundwater: Making the invisible visible.* Paris: UNESCO.

Wang, H., Jiang, X.-W., Wan, L., Han, G., & Guo, H. (2015). Hydrogeochemical characterization of groundwater flow systems in the discharge area of a river basin. *Journal of Hydrology*, 527, 433-441. doi: **https://doi.org/10.1016/j.jhydrol.2015.04.063**

Yang, P., Luo, D., Hong, A., Ham, B., Xie, S., Ming, X., Wang, Z., Pang, Z. (2019). Hydrogeochemistry and geothermometry of the carbonate-evaporite aquifers controlled by deep-seated faults using major ions and environmental isotopes. *Journal of Hydrology*, 579, 124116. doi: **https://doi.org/10.1016/j.jhydrol.2019.124116**

Zainol, N. F., Zainuddin, A. H., Looi, L. J., Aris, A. Z., Isa, N. M., Sefie, A., & Yusof, K. M. (2021). Spatial Analysis of Groundwater Hydrochemistry through Integrated Multivariate Analysis: A Case Study in the Urbanized Langat Basin, Malaysia. *International Journal of Environmental Research and Public Health*, 18(11), 5733. doi: **https://doi.org/10.3390/ijerph18115733**

Zeng, J., Yue, F.-J., Li, S.-L., Wang, Z.-J., Wu, Q., Qin, C.-Q., & Yan, Z.-L. (2020). Determining rainwater chemistry to reveal alkaline rain trend in Southwest China: Evidence from a frequent-rainy karst area with extensive agricultural production. *Environmental Pollution*, 266(3),115166. doi: **https://doi.org/10.1016/j.envpol.2020.115166**